공학석사 학위논문

Electrochemical Analysis of Membrane Electrode Assembly Applied with Nitrogen Functionalized Electrocatalyst for Polymer Electrolyte Membrane Fuel Cell

질소처리 촉매가 적용된 고분자전해질연료전지

막-전극 접합체의 전기화학적 분석 및 평가

2020년 8월

서울대학교 대학원

공과대학 화학생물공학부 에너지환경화학융합기술전공

김용민

Electrochemical Analysis of Membrane Electrode Assembly Applied with Nitrogen Functionalized Electrocatalyst for Polymer Electrolyte Membrane Fuel Cell

지도 교수 성 영 은

이 논문을 공학석사 학위논문으로 제출함
2020 년 06 월

서울대학교 대학원
공과대학 화학생물공학부 에너지환경화학기술융합전공
김용민

김용민의 석사 학위논문을 인준함
2020 년 06 월

위 원 장   최 장 욱   (인)

부위원장   성 영 은   (인)

위   원   이 규 태   (인)

Abstract

Electrochemical Analysis of Membrane Electrode Assembly Applied with Nitrogen Functionalized Electrocatalyst for Polymer Electrolyte Membrane Fuel Cell

Yong Min Kim

School of Chemical & Biological Engineering

Chemical Convergence for Energy & Environment

The Graduate School

Seoul National University

Polymer electrolyte fuel cell (PEMFC) is an energy conversion device that exploits chemical energy of hydrogen and oxygen to produce electricity for automotive and stationary applications. They are highly preferred among the sustainable energy sources since no pollutants need to be produced and energy production and storage is highly efficient. However, there are limitations to the complete transition to the hydrogen energy system with current PEMFC technology, one of them being the scarcity and high price of

platinum and catalyst durability. Many researches are thus being made to minimize the amount of platinum while maximizing the oxygen reduction reaction (ORR) activity and durability. State-of-art catalysts include Pt-based transition metal bimetallic alloy with core-shell structure, ordered array, distinctive 3D structure, etc. These electrocatalysts have well displayed enhanced ORR activity and durability and opened new windows for improved PEMFC electrodes.

However, the high ORR activity and durability based on liquid-electrolyte half-cell is not often translated to actual PEMFC performance in single-cell operating conditions. These gaps come from the difference in electrode configurations, such as electrode structure, ionomer distribution and thickness, membrane hydration, conductivity, etc. Oftentimes, even the most improved electrocatalysts that show excellent activity in a half-cell fails to translate its performance in single-cell environment. It is thus crucial to examine the behavior of novel electrocatalysts in a single-cell operating condition and make adequate considerations in the design of the catalyst synthesis method and procedure.

This thesis focuses on employing a novel catalyst that uses soft-nitriding technique to functionalize the carbon support of Pt/C catalyst with nitrogen to single-cell PEMFC to analyze its behavior and performance on actual fuel cell operating conditions. Membrane electrode assembly (MEA) was fabricated using a catalyst-coated membrane (CCM) method to perform the

analysis. As a result, the single cell performance was proven to improve in a single-cell level, showing a noticeable increase in activation polarization region. Such result was analyzed to have derived from enhance ionomer distribution and thus improved proton conductivity and triple-phase boundary formation of the new electrode. On the other hand, the compressed electrode thickness and increased hydrophilicity was degenerated the mass transfer in the high-voltage region. The performance nevertheless outperformed the conventional type of electrode throughout the entire voltage region. Enhance performance was also shown in diverse relative humidity and backpressure conditions, and accelerated stress test proved the improved durability of the catalyst.

From the single-cell application and characterization, the compatibility of the novel N-functionalized Pt/C catalyst in actual PEMFC operating conditions have been confirmed. It was also shown that the new soft-nitriding technique can be helpful for designing new catalysts that can well perform in the single-cell level.

Keywords: Polymer electrolyte membrane fuel cells (PEMFCs), Oxygen reduction reaction, N-functionalization, membrane-electrode assembly (MEA).

Student Number: 2018-29625

Contents

List of Tables

List of Figures

Chapter 1. Introduction

1.1   Fuel Cells : General Introduction

1.1.1   Theoretical basis of fuel cell

Fuel cells are defined as electrochemical energy conversion devices that directly convert chemical energy to electrical energy.[1-3] The idea of fuel cell was first introduced by Sir William Grove in 1839.[4] Grove experimentally demonstrated the concept of hydrogen fuel cell by immersing two platinum electrodes in a solution of sulfuric acid, and separately sealing the opposite two ends in oxygen and hydrogen, respectively. He found a constant current flowing through the primitive hydrogen fuel cell. Diverse types of fuel cells utilizing methanol, formic acid, etc. have been developed since then, but hydrogen fuel cells are still the most commonly researched and commercialized type.

Hydrogen fuel cells are mainly composed of electrolyte, current collector, fuel distribution channels and two distinctive electrodes, anode and cathode. (Figure 1.1) Two different electrochemical reactions are driven by the gap between the redox potential of two gases in each of the electrodes. Hydrogen oxidation reaction in the anode and oxygen reduction reaction in the cathode take place as shown below.

Anode :	$H_2 \rightarrow 2H^+ + 2e^-$	$E^0 = 0.000V$
Cathode :	$\frac{1}{2} O_2 + 2H^+ + 2e^- \rightarrow H_2O$	$E^0 = 1.229V$
Overall :	$H_2 + \frac{1}{2} O_2 \rightarrow H_2O$	$E^0 = 1.229V$
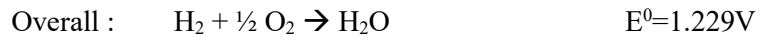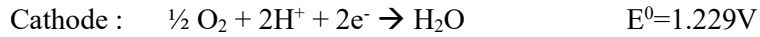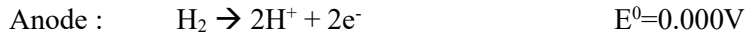
Various types of hydrogen fuel cells have been developed according to different electrolyte types. (Table 1.1)

Polymer electrolyte membrane fuel cell (PEMFC) is unquestionably the most widely used and favored type for transportation, residential power systems, and portable electronic devices. Its advantages over other types of fuel cells vary, from low operating temperature to high power density, long durability, and short start-up time. PEMFCs are based on polymer electrolyte membranes, which is composed of polymer backbones with acid-based side-chain groups forming a network for proton conduction.[3, 5] The most renowned and widely used membranes are Nafion membrane from Dupont. Nafion membranes are closed to ideal in its properties of high ionic conductivity, low electronic conductivity, low cost, and high mechanical, chemical stability. Protons generated in the anode by hydrogen oxidation reaction (HOR) travel through the polymer membrane to the cathode, while electrons are passed via external circuit to the same destination where oxygen reduction reaction (ORR) occurs.
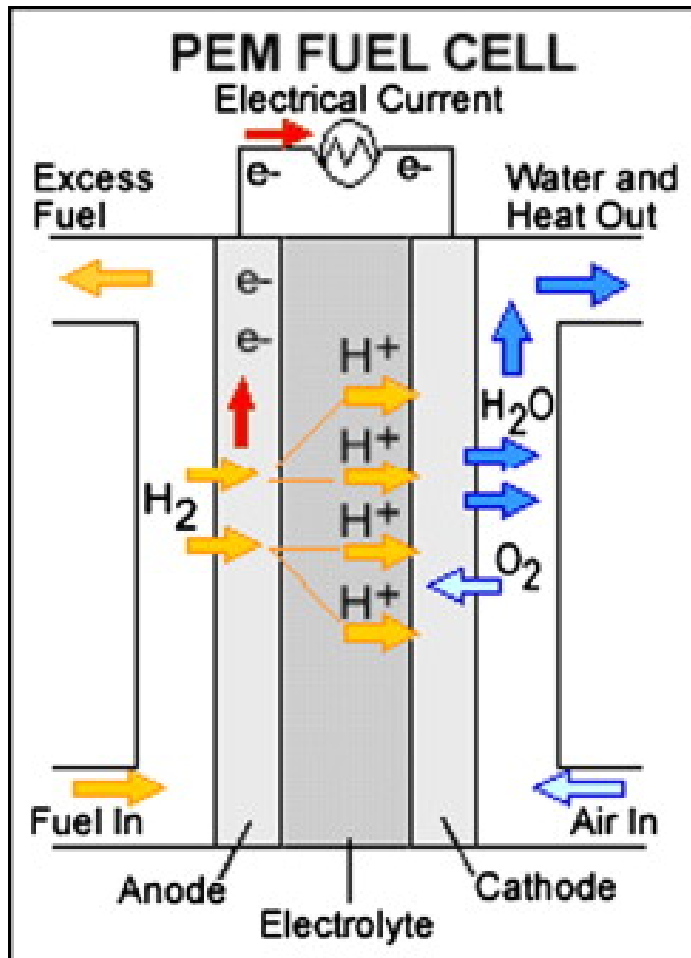
Figure 1.1 Schematic representation of PEMFCs single cell [3]

Table 1.1. Types of different fuel cells [1]

	PEMFC	PAFC	AFC	MCFC	SOFC
Electrolyte	Polymer membrane	Liquid H_3PO_4	Liquid KOH	Molten Carbonate	Ceramic
Charge Carrier	H^+	H^+	OH^-	CO_3^{2-}	O^{2-}
Operating Temperature	80ºC	200ºC	60-220ºC	650ºC	600-1000ºC
Catalyst	Platinum	Platinum	Platinum	Nickel	Perovskites (Ceramic)
Cell Components	Carbon-based	Carbon-based	Carbon-based	Stainless-based	Ceramic-based
Fuel Compatibility	H_2, Methanol	H_2	H_2	H_2, CH_4	H_2, CH_4, CO

In the process of producing electricity, four major steps take place within the fuel cell unit: reactant gas transport into the fuel cell, electrochemical reaction on the surface of two electrodes, proton conduction through the membrane and electron transfer through external circuit, and finally product removal from the fuel cell.[1] Cell components and their respective roles in each step is described in the next section.

1.1.2   Cell Components

A PEMFC single cell is mainly composed of a membrane, catalyst layers, gas diffusion layers (GDL), and biopolar plates usually containing gas flow fields. Schematics of a single cell PEMFC and each of its components are shown in Figure 1.2.

Membrane

In a PEMFC, polymer electrolyte membrae is used as the electrolyte medium. Protons generated as products of hydrogen oxidation reaction in the anode transports through the membrane. Gas phases from both sides, on the other hand, are hindered from permeating through the membrane which acts as a seperator. Electrons are also insulated by the membrane and are not allowed to travel through, and thus are forced to be conducted through an external circuit.[1, 3] Nafion® (Dupont) is the most widely used type of

membrane in the world of PEMFC. It contains a structure of polytetrafluoroethylene (PTFE) which acts as a backbone, and functional groups consisting of sulfonic acids. (Figure 1.3.) Sulfonic acid functional groups bind proton easily and are used as proton conduction sites.

Vehicular diffusion method and hopping mechanism are the generally accepted proton conductino mechanisms. In vehicular diffusion, protons are combined with water to form hydronium ions and are carried by the water flow across the membrane. Hopping mechanism states that protons jump from one proton adsorption site to another within the membrane structure, especially when sulfonic functional groups are connected to each other by sufficient hydration.[6]
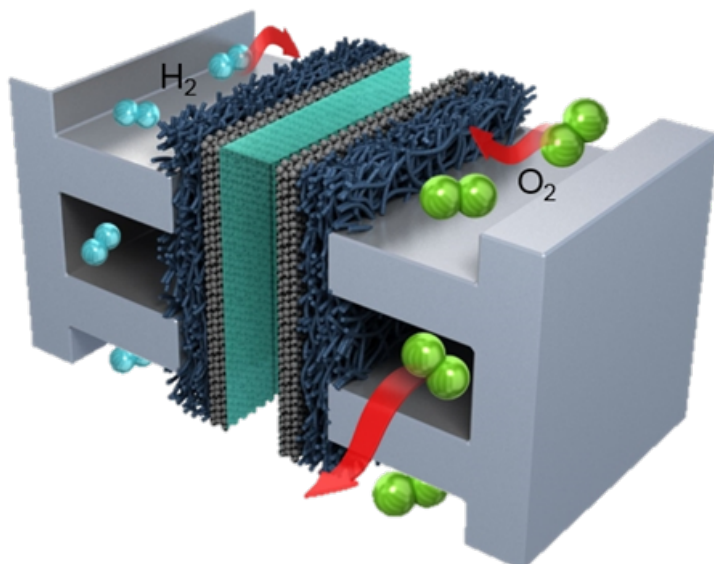
Figure 1.2 Polymer Electrolyte Membrane Fuel Cells Cell Components [7]
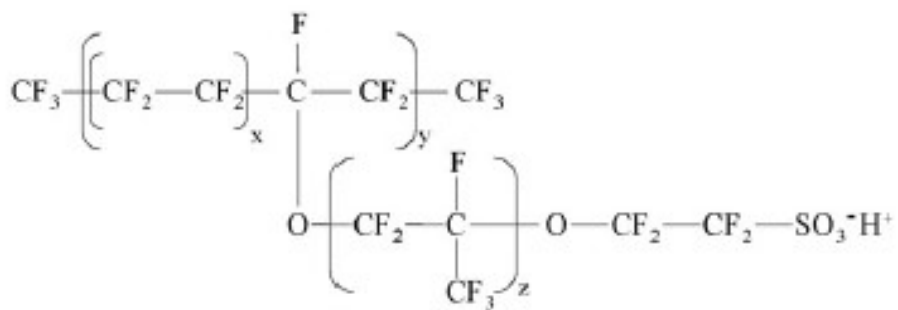
Figure 1.3 Chemical structure of Nafion membrane [8]

Catalyst layer

Catalyst layers are coated on each side of the membrane. Catalyst layers are places of electrochemical reactions, and are composed of catalyst, ionomer, and gas diffusion spaces.[3] On the anode side, hydrogen oxidation reaction occurs and on the cathode side, oxygen reduction reaction takes place. Each of the electrochemical reaction is carried in sites named triple phase boundary (TPB). TPB is where three phases (gas, proton, and catalyst site) meets. Proton conduction and gas diffusion to the reaction site are thus crucial. Well dispersed ionomers act as proton conduction pathways and at the same time provides void spaces for gas diffusion. An illustration of catalyst layer with ionomer well dispersed to form TPB is shown in Figure 1.4.

For the process of electrochemical reaction, protons are transported in/out of catalyst layer to/from the membrane via nafion ionomers. Secondly, electrons are conducted to/from the catalyst reaction site through the external circuit, bipolar plate, and gas diffusion layer. Finally, gases are provided through the flow field and gas diffusion layer.[9]

To minimize charge transfer resistance, catalyst layer should be closely bound to the membrane. A widely used technique is call the catalyst-coated membrane (CCM) method, of which catalyst inks are directly applied and coated to each side of the membrane.

The most widely researched and commercialized catalysts are based on platinum. Platinum serves as an excellent catalyst for hydrogen oxydation reaction and oxygen reduction reaction, located at the top of the ORR volcano plot among single atom catalysts. The disadvantage of using platinum comes from its scarcity and high cost. Developments of platinum catalysts have thus been made by applying carbon supports and loading platinum nanoparticles on the surface of the supports, minimizing the platinum usage and maximizing surface area.[10] Until now, developing high activity, durable, and cheap electrocatalysts are key area of research in PEMFC.

One most common technique being vigorously researched to improve Pt/C catalysts is doping nitrogen species on the surface of carbon support. Diverse technologies including ammonia annealing[11-14], nitric acid treatment[15, 16], dopamine coating[17, 18] and others[19-22] have been introduced. Many researches have reported the enhanced catalytic activity or enhanced ionomer distribution due to such research. However, improvement on both the catalyst activity and single cell performance has not yet been vigorously reported.
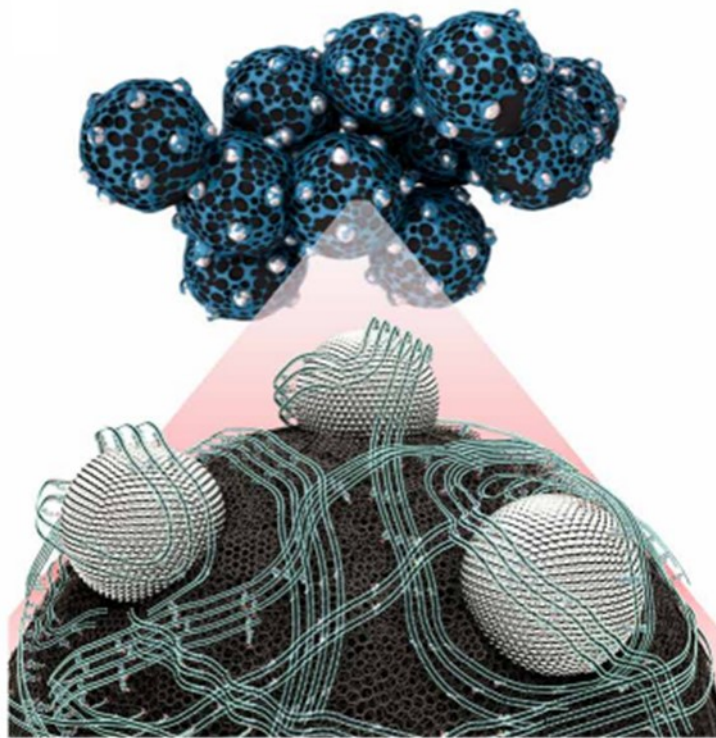
Figure 1.4 Illustration of the catalyst layer showing Pt/C catalysts covered with polymer electrolyte ionomer [23]

Gas diffusion layer (GDL)

Gas diffusion layer (GDL) is applied to diffuse gas from the flow field to the catalyst layer, remove generated water, and conduct electrons from/to the catalyst layers.[3] They are composed of porous carbon fiber layer, called micro-porous layer (MPL), which is pressed on a carbon paper. GDL not only acts as gas distribution and electron transport material, but also provides mechanical support to the MEA. They are important factors of mass transfer, and their high porosity reaching 80% allows efficient transport of reactants into the reaction sites of the catalyst layers in the though-plane direction.[24] The MPL structure provides large surface area for a good contact and thus a minimum surface resistance between the catalyst layer and GDL. The carbon papers are usually treated with polytetrafluoroethylene (PTFE), which is very hydrophobic. Such treatment helps remove generated water from the catalyst layer and prevent flooding.

Bipolar plate

Bipolar plates serve as reactant gas and product passage channel, electron conductor, and provide mechanical support to the MEA. Bipolar plates are composed of materials with high heat and electron conductivity to efficiently connect the two electrodes electrically and remove heat. They are also generally engraved with flow fields that distributes reactant gas and

remove generated water products.[25] Classic types of flow fields are parallel, serpentine and integrated type flow fields.[26, 27] They are composed of gas channel that provides gas and water pathway and ribs that are connected to the GDL and provide electrical connection. Relatively new types of flow fields including porous metallic powder, micro-coil, and metal foam have recently been under research to improve mass transport and water management in fuel cells.[25, 28-30]

1.1.3   Performance Losses of PEMFCs

The overall performance of PEMFC is affected by the voltage losses, called overpotentials, over the current range of the cell as shown in Figure 1.5. The equilibrium voltage (E_0) of 1.229V is compensated by three types of losses, which are activation, ohmic, and concentration overpotentials.[31]

$$E = E_0 - \eta_{act} - \eta_{ohmic} - \eta_{conc}$$

Activation overpotential (η_{act}) accounts for the reaction kinetics of the catalyst. Ohmic overpotential (η_{ohmic}) arises from charge transfer resistance of proton and electrons. Concentration overpotential (η_{conc}) is related to reactant diffusion limitations from the bulk to the reaction site.[32]

Activation overpotential is caused by reaction kinetics on the surface of catalysts. Low catalytic activity and slow reaction kinetics cause voltage losses, and thus this type of overpotential is largely dependent on the most sluggish reaction step.[33, 34] Activation overpotential occurs at low current density region, and is generally governed by the Butler-Volmer equation or its simplified form, Tafel equation.

$$\eta_{act} = RTlnj_0/\alpha nF + RT/\alpha nF \log j \ ^{32}$$

$$j_0 = nFC_Rf_1e^{-\Delta G1/(RT)}$$

As shown in the equation, high exchange current density (j_0) results in a low activation overpotential. High temperature, low activation barrier, and high reactant concentration all accounts for minimizing the activation overpotential.

Ohmic overpotential is based on incomplete ionic and electronic conductivity of the cell components which causes resistance in charge transfer over the cell. Its effect is dominantly shown in the mid-current region and is explained by the equation below.
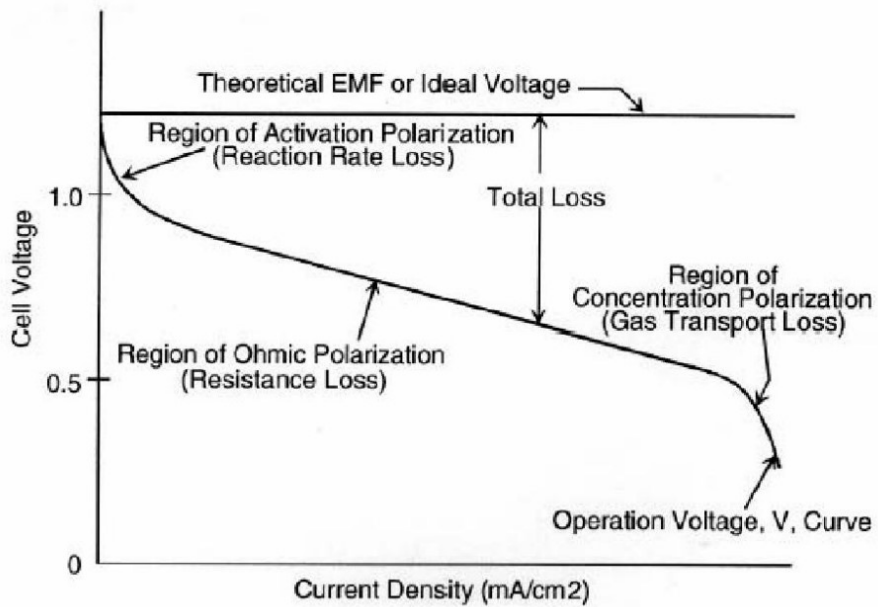
Figure 1.5. Typical fuel cell polarization curve [35]

$$\eta_{ohmic} = iR_{ohmic}$$

Cell internal resistance (R_{ohmic}) is composed of membrane resistance, electrical resistance, surface resistance due to incomplete contact between cell components, etc. [33, 36]

Concentration overpotential occurs when the diffusion of reactant gas to the reaction site is insufficient to meet the stoichiometric amount required for cell reaction.

$$\eta_{conc} = RT/\alpha nF \ln j_L/(j_L-j) \text{ [1]}$$

$$j_L = nFD_{eff}C_R/\delta$$

High limiting current density (j_L) results in a low concentration overpotential, and such can be achieved by accomplishing high effective reactant diffusivity (D_{eff}), high reactant concentration (C_R), and low electrode thickness (δ). Water management and loading amount of catalyst are thus important factors affecting concentration overpotential.

1.2　Challenges of PEMFCs

To enhance the performance and durability of PEMFC, diverse researches have been conducted to find new electrocatalysts to enhance electrode reactions. Among the two electrochemical reactions that take place in PEMFC, ORR is considered much more critical than HOR due to its slow kinetics and thus high impact on activation overpotential. In ORR, four electrons participate in the reaction and the reaction steps and mechanism are much more complex. The strong bonding of the oxygen atoms is hard to break, and oxide formations and hydrogen peroxide side product generation all account for the sluggishness of the reaction.

Platinum group metals (Pt, Pd) are considered as the best materials for ORR catalysis and many catalysts based on these materials have been developed.[37, 38] However, these materials are scarce in nature and are poor in durability, limiting the wide commercialization of PEMFC products and thus enhanced ORR activity and durability catalysts have been a hot research topic over the decade.[39] Many groups over the past years have reported high-performance, high-durability ORR electrocatalysts over the years. However, applying them to full cell and actuating the elevated performance is another challenge.

Unlike liquid half-cell performance, single cell performance is affected by various factors such as electrode structure, ionomer distribution and

thickness, membrane hydration, conductivity, etc. Oftentimes, even the most improved electrocatalysts that show excellent activity in a half-cell fails to translate its performance in single-cell environment.[40, 41] Therefore, examining the catalyst performance in single cell environment and improving the cell components to and optimal degree should be considered as important. Moreover, single-cell parameters should also be considered and adjustments to the manufacturing method or process should be made accordingly when developing a novel catalyst.

1.3   Aim of this Thesis

Diverse techniques to improve platinum based catalysts have been reported to improve ORR activity of PEMFC catalysts. Various nitrogen-group functionalization methods of the catalyst or carbon support have been one of them, and many studies have succeeded in ORR catalysis enhancement and some of them have reported actual increase in PEMFC single cell performance. However, most of these methods utilize NH_3 and require high temperature annealing in the synthesis process. Drawbacks coming from this is that NH_3 is innately toxic and high temperature treatment of catalyst may affect the carbon support properties.

Soft-nitriding is a recently reported method to grow in situ ligand-free nanoscale noble metal catalysts, such as Au, Pd, and Pt, onto carbon.[42] The method uses a low temperature urea pretreatment to enrich nitrogen species on the surface of carbon supports. Urea, unlike NH_3, is less toxic and environmentally friendly and cost-effective to use. The nitriding process is also greatly simplified, making the process efficient in an engineering point of view.

In this study, the soft-nitriding technique was exploited to modify the carbon support of the platinum-based electrocatalyst. Half-cell test revealed that the ORR activity of the novel electocatalyst greatly

improves compared to that of the untreated catalyst. To translate the enhanced activity in the liquid electrolyte half-cell to the elevation of the single cell performance in a PEMFC operating condition, membrane-electrode assembly (MEA) was produced using the spray coating method. The changes in electrode structure caused by the nitrogen pretreatment and the mechanisms of such change was closely examined to produce an optimized electrode for single-cell performance realization. Both physical and electrochemical measurements were used, including scanning electron microscopy (SEM), contact angle analysis, i-V polarization, electrochemical impedance spectroscopy (EIS), cyclic voltammetry (CV), etc. The optimized single-cell was tested in different operating conditions with varying relative humidity and fuel backpressure. Finally, the durability of the electrode was accessed by conducting an accelerated stress test.

Chapter 2. Experimental

2.1 Synthesis of Platinum/Soft-Nitrided Vulcan Carbon electrocatalyst

Soft-nitriding method has been well reported by Liu et al. [42] Vulcan XC-72 (Fuel Cell Store) was used as carbon support material and was grinded physically with urea (99.0%, Samchun) and sealed. The mixture is annealed at 150°C and 300°C for 2h each, and then washed with water and ethanol to remove any remaining urea. The synthesized N-functionalized carbon powder was well dried at 60°C until next step.

Platinum particles were deposited via polyol reduction method.[43] $H_2PtCl_6 \cdot 6H_2O$/EG was used as a precursor to produce platinum nanoparticles. Platinum nanoparticle amount corresponding to 40 percent of total catalyst weight was deposited on N-functionalized Vulcan XC-72 (NVC) and Vulcan XC-72 (VC) respectively. After solution filtering and sufficient washing with DI, synthesized catalyst filter cake was well dried in vacuum oven for 24h before use. The schematic of catalyst synthesis is shown in Figure 2.1.

Polyol Reduction

Pt - Glycolate compound reduction

Vulcan XC-72 Carbon

Soft-nitriding   *Urea annealed in 300 ℃*

Platinum on Vulcan XC-72 Carbon (Pt/VC)

N-doped Vulcan XC-72 Carbon

Polyol Reduction

Pt - Glycolate compound reduction

Platinum on N-doped Vulcan XC-72 Carbon (Pt/NVC)
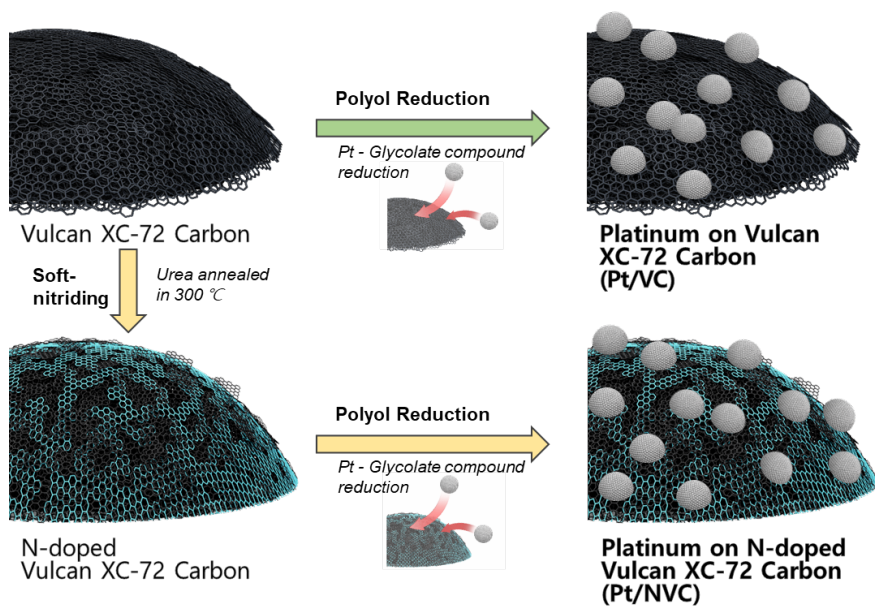
Figure 2.1. Schematic of Pt/NVC, Pt/VC catalyst synthesis

2.2 Electrocatalyst characterization

The morphology of synthesized electrocatalyst was analyzed using analytical transmission electron microscopy (Analytical TEM, Tecnai F20). The loading amount of platinum was confirmed by thermos-gravimetric analysis (TGA, TA SDT Q600). Liquid electrolyte half-cell analysis using rotating disk electrode was used to assess the ORR activity and mass activity of the catalysts.

2.3. Membrane-electrode assembly (MEA) preparation

Membrane-electrode assembly (MEA) of $5cm^2$ was prepared by the catalyst-coated membrane (CCM) method. Catalyst ink composed of anode/cathode electrocatalyst, D.I. water, 2-propanol (Sigma Aldrich), and Nafion solution (Sigma Aldrich) was prepared and well sonicated for 1hr. 40wt% Pt/C (Johnson Matthey) was used as anode catalyst and synthesized 40wt% Pt/NVC or 40wt% Pt/VC catalysts were applied to the cathode. The catalysts were then spray-coated to Nafion 212 (Dupont) membrane with loading amount of 0.2 mg_{pt} cm^{-2} on both anode and cathode. The CCMs were dried at room temperature for overnight then assembled using gas-diffusion layer (JNT-60-A3) and Teflon gasket (250μm).

2.4. Physical characterization of membrane-electrode assembly

The electrode morphology and thickness were analyzed using field emission scanning electrode microscopy (FE-SEM, MERLIN Compact). Contact angle analyzer (Pheonix MT(M)) was used to analyze the hydrophilicity of the electrodes. D.I. water droplets were applied to the surface of the electrodes and the average contact angle of the droplets from the side view was used to compare the relative hydrophilicity of each electrode.

2.5. Electrochemical characterization of membrane electrode assembly

The MEAs were put into a single cell with a serpentine flow field and were supplied with 150ml min^{-1} H$_2$ on the anode side and 800ml min^{-1} air on the cathode side with 50% relative humidity. The cell temperature was set as 80°C.

i-V polarization test was conducted with a scan rate of 0.05 A s^{-1}. Electrochemical impedance spectroscopy (EIS) (IM-6, Zahner) was recorded in galvanic mode of 0.8, 0.6, and 0.4V state and the AC current was applied with 5 mV. The frequency range was set to 100mHz to 100kHz. Cyclic voltammetry (IM-6, Zahner) was then conducted in a H$_2$, N$_2$ environment to

confirm the electrochemically active surface area. Complex capacitance analysis was made on the same environment by conducting the EIS experiment in 0.45V condition, in which no faradaic reaction, including hydrogen adsorption/desorption and Pt oxide formation, in the electrode occurred as confirmed by the cyclic voltammetry result.

To study the single-cell performance in diverse operating conditions, the polarization test was conducted in relative humidity of 0, 20, 40, 60, 80, and 100%. The backpressure test was also conducted in 0, 0.5, 1.0, and 1.5 bar pressurized condition.

To test the durability of each electrode, i-V cycling in 80°C and 50% relative humidity H_2 and air was conducted for 70 hours. The polarization curves and EIS, CV results were then recorded to be compared with the initial state.

Chapter 3. Results and discussion

3.1. Electrocatalyst Characterization

XPS analysis was conducted to characterize the carbon support surface after soft-nitriding. The results as shown in Figure 3.1.1 denotes that NVC sample was well nitrided on the surface with pyrrolic nitrogen species dominating the surface functional groups. Pyrridinic and quaternary nitrogen species were also detected.

The synthesized Pt/NVC and Pt/VC electrocatalysts were examined using analytical TEM as shown in Figure 3.1.2 and its platinum loading of 40 weight percent was confirmed by TGA analysis as in Figure 3.1.3. TEM image showed that both the Pt/NVC and Pt/VC catalysts had evenly distributed platinum particles of diameter averaging 4nm on carbon supports. Their platinum loading amount was equivalent to 40% of the total catalyst weight as intended in the synthesis procedure.

Liquid half-cell analysis was finally conducted to assess the ORR activity of the novel catalyst. Figure 3.1.4 shows that the Pt/NVC catalyst exerts enhanced ORR activity in terms of onset potential and limiting current density. Mass activity comparison of commercial Pt/C 40% (Johnson Matthey) and the two synthesized catalysts is also depicted in Figure 3.1.5.
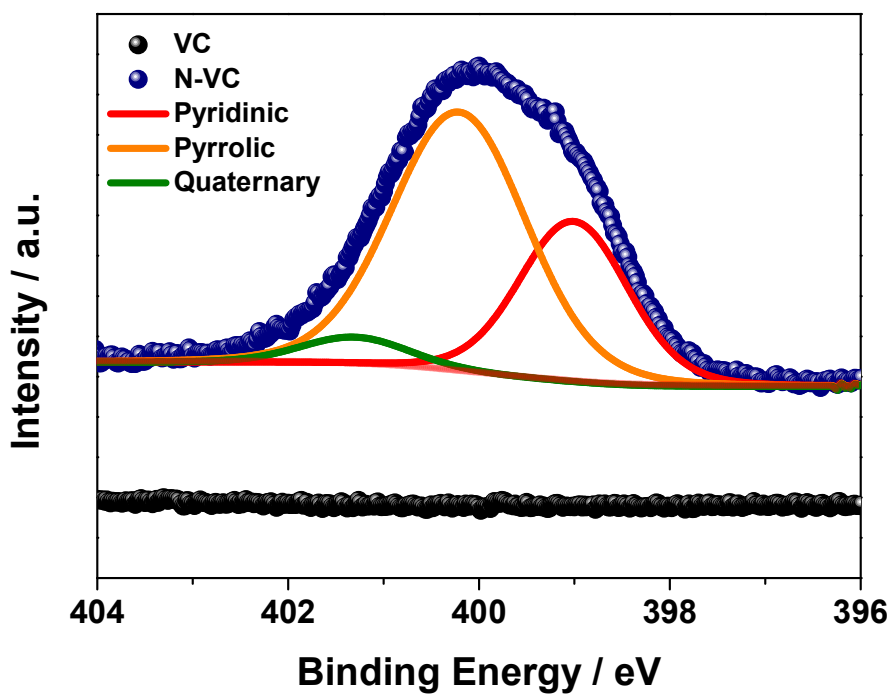
Figure 3.1.1. XPS analysis of soft-nitrided carbon support (NVC)
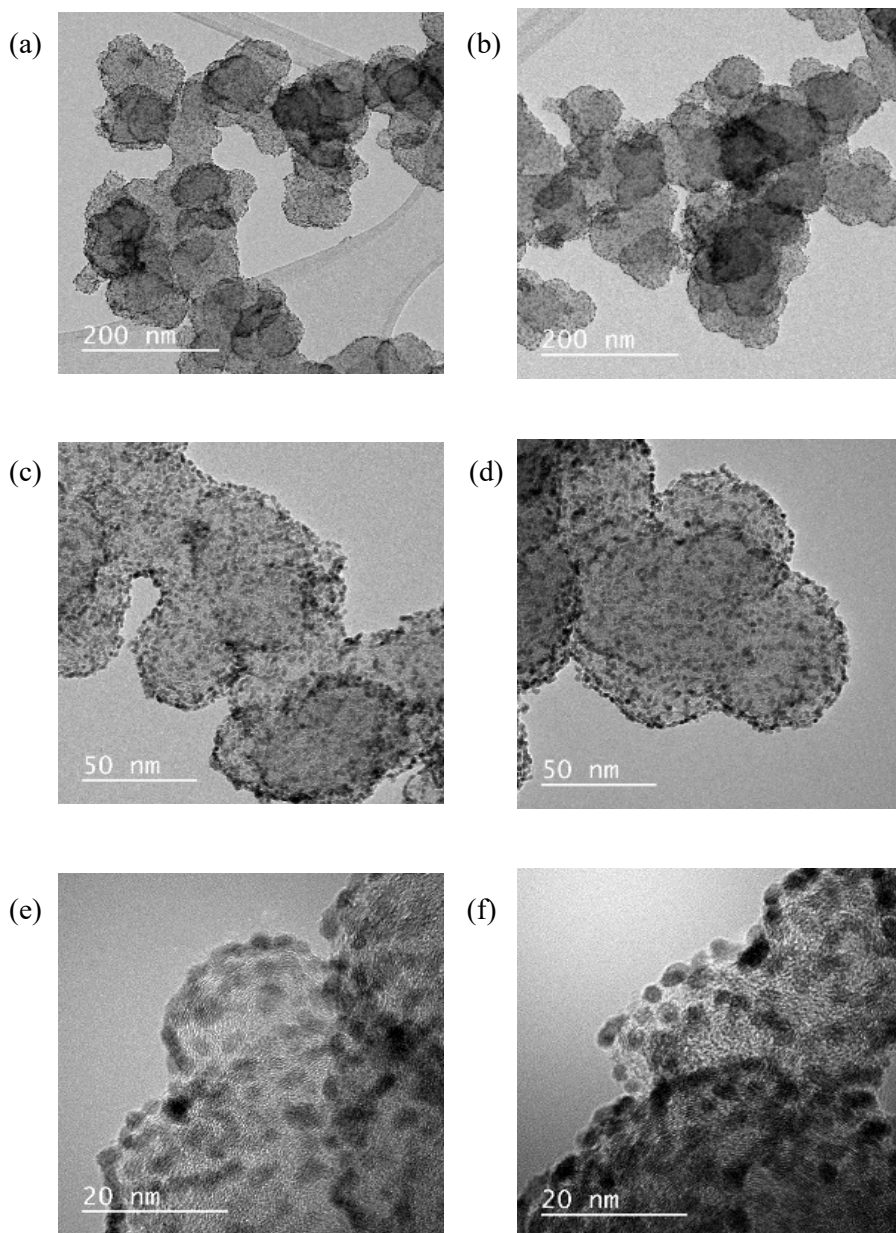
Figure 3.1.2. TEM images of synthesized electrocatalysts (a), (c), (e) TEM image of Pt/NVC catalyst, (b), (d), (f) TEM image of Pt/VC catalyst
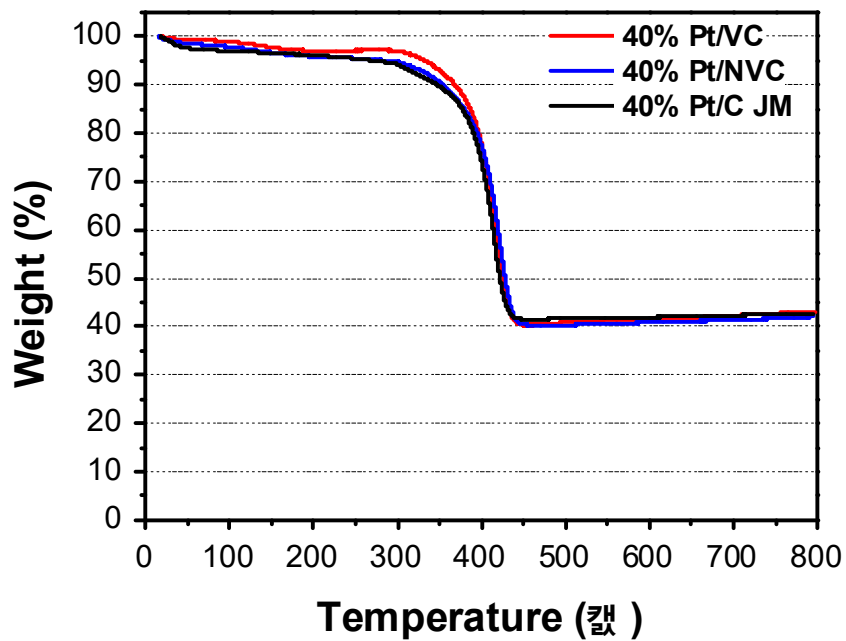
Figure 3.1.3. TGA analysis of synthesized and commercial 40 wt% Pt electrocatalysts.
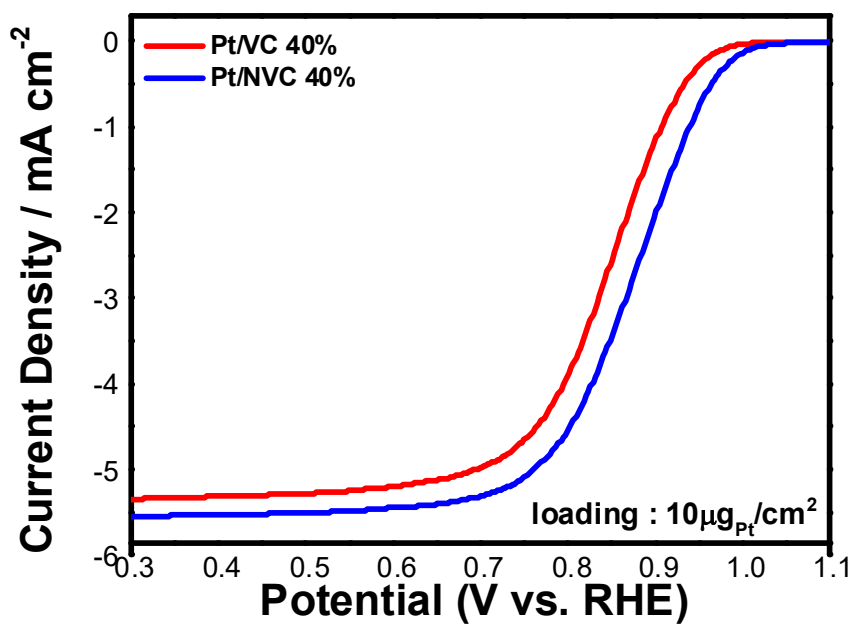
Figure 3.1.4. Liquid electrolyte half-cell analysis of ORR activity of synthesized electrocatalysts
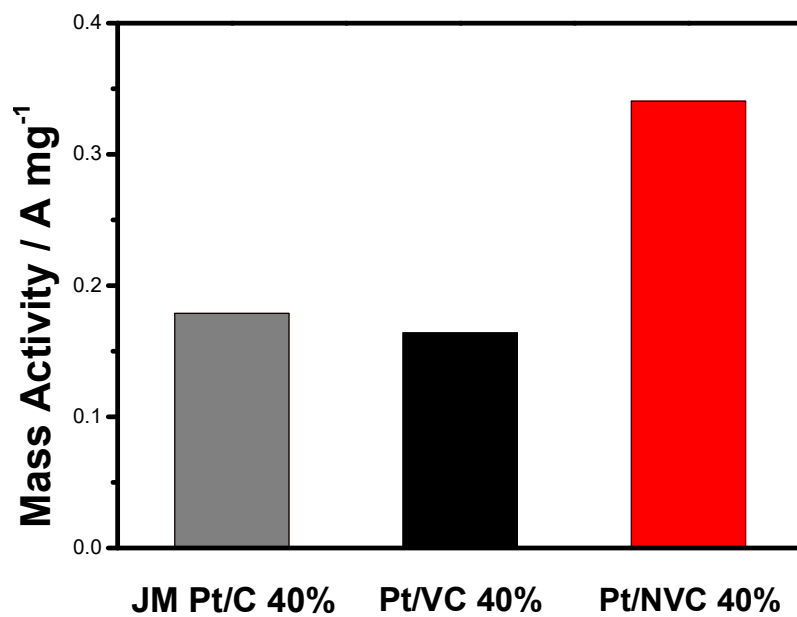
Figure 3.1.5. Liquid electrolyte half-cell ORR mass activity

3.2 MEA Characterization

MEAs using commercial Pt/C 40% (Johnson Matthey) as the anode catalyst and synthesized Pt/NVC 40%, Pt/VC 40% catalysts as the cathode catalysts were manufactured using the CCM method. Physical characterization of the MEA and electrochemical diagnosis were conducted on the single-cell level to test the performance and characteristics of the electrode composed of the novel electrocatalyst.

3.2.1. Physical characterization

The field-emission scanning electron microscopy was conducted on the surface and cross-section of the MEA as shown in Figure 3.2.1. and 3.2.2. The surface of the Pt/NVC 40% electrode appeared to be very well distributed and smooth. No particular agglomeration of the ionomer or catalyst were depicted. On the other hand, the Pt/VC 40% electrode showed inferior morphology to Pt/NVC 40% electrode. The electrode was far from smooth and agglomerates of Nafion ionomer in the form of dendrites and uncovered Platinum particles shown as white, glimmering spots were identified. The cross-section of the two electrodes differed as shown in Table 3.2.1. The Pt/NVC 40% electrode showed a 4.6μm of thickness in average, while the Pt/VC 40% electrode was in average 5μm thick.

From the FE-SEM analysis, it could be suspected that the ionomer

distribution of the Pt/NVC sample had been improved, resulting in a more uniform electrode structure with ionomer well covering the Platinum nanoparticles evenly. This had been a logical conclusion since previous reports by Ott. et al. and Orfanidi et al. have shown that nitriding of the carbon supports can result in better interaction between the Platinum-based catalysts and Nafion ionomers, enhancing the electrode structure.[16]

(a) x10k magnified image

(b) x30k magnified image

(c) x10k magnified image

(d) x30k magnified image
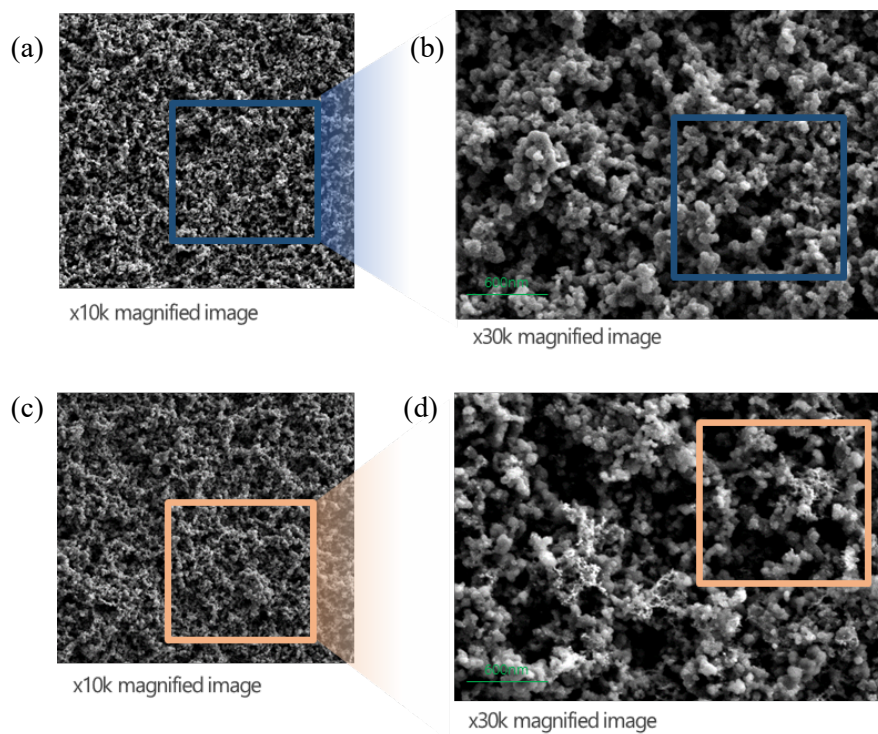
Figure 3.2.1. Field Emission Scanning Electron Microscope image of Electrode Surface (a) 10,000, (b) 30,000 times magnified image of Pt/NVC 40% electrode, (c) 10,000, (d) 40,000 times magnified image of Pt/VC 40% electrode

(a)

H 1 = 4.689 µm

(b)

H 1 = 5.324 µm
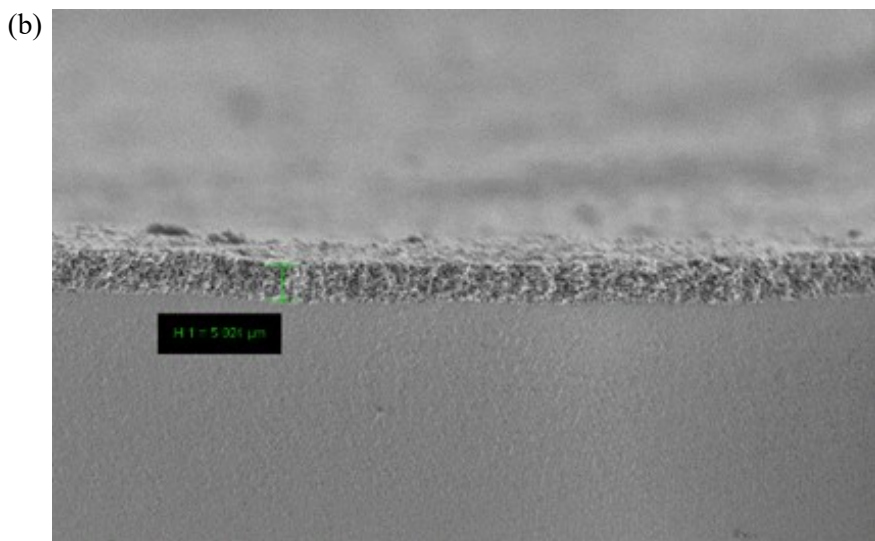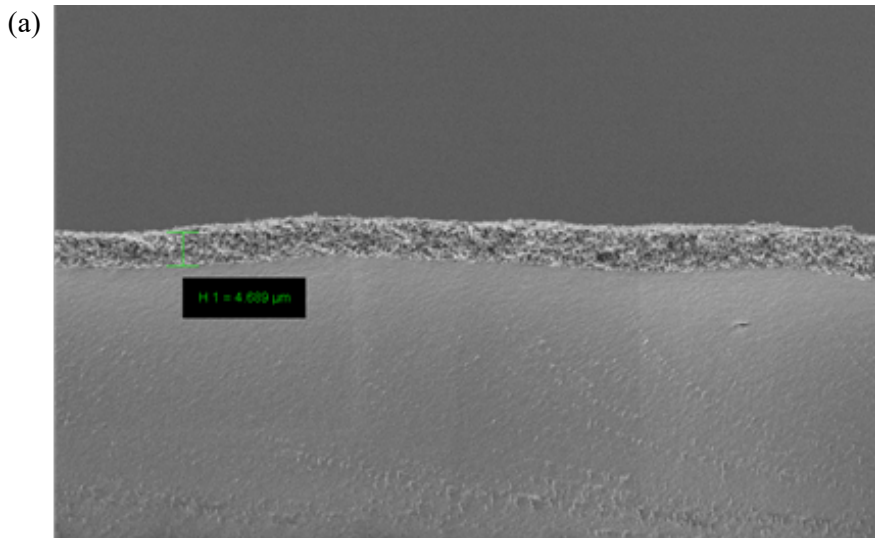
Figure 3.2.2. Field Emission Scanning Electron Microscope image of electrode cross-section (a) Pt/NVC 40% electrode, (b) Pt/VC 40% electrode

Table 3.2.1. Thickness comparison between electrodes

Div.	Electrode Thickness (μm)
Pt/NVC 40%	4.689
Pt/VC 40%	5.024

From the contact-angle analysis, the hydrophobicity of the two electrodes could be determined. The contact angle of Pt/NVC 40% electrode was 129.30º, while for Pt/VC 40% electrode it was 138.49º as shown in Figure 3.2.3. and Table 3.2.2. It could be concluded that the hydrophilicity of the Pt/NVC 40% electrode was greater than that of Pt/VC 40% electrode. It could be expected that the water management and further the mass transport of the Pt/NVC 40% electrode could be compromised to a certain extent due to such physical property.
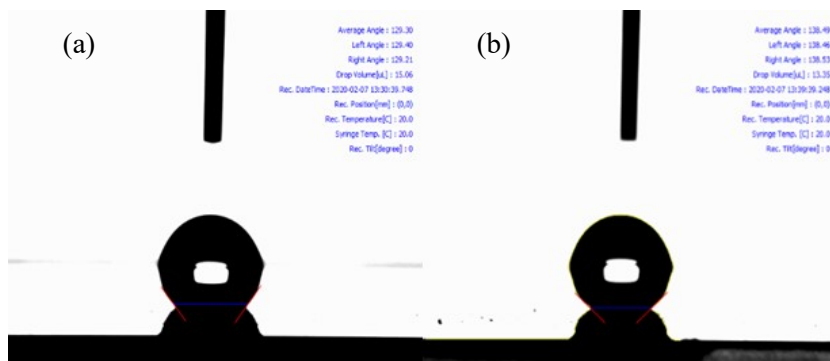
Figure 3.2.3. Contact angle analysis (a) Pt/NVC 40% electrode, (b) Pt/VC 40% electrode

Table 3.2.2. Contact angle comparison between electrodes

Div.	Contact Angle (^{0})
Pt/NVC 40%	129.30
Pt/VC 40%	138.49

3.2.2. Electrochemical characterization

Electrochemical analysis of the MEA applied with Pt/NVC 40% and Pt/VC 40% catalysts were conducted on a single cell level to test their performance and behavior in actual PEMFC operating environment.

Single-cell performance

The Pt/NVC 40% and Pt/VC 40% catalysts were applied to MEA and their performance was tested on a single-cell level by current-voltage polarization in 50% relative humidity and 80°C temperature. The polarization result of Pt/NVC 40%, Pt/VC 40%, with the performance of commercial Pt/C 40% (Johnson Matthey) for comparison are shown in Figure 3.2.4. The current density at 0.8, 0.6, 0.4V, each representing activation, ohmic, mass transfer polarization region, are shown in Table 3.2.3. It can be seen from the polarization curve that the performance of the Pt/NVC 40% electrode shows an especially improved performance in the high-voltage region, representing enhanced electrode activation. Such improvement can also be seen in the electrochemical impedance spectroscopy result shown in Figure 3.2.5.

(a)

(b)
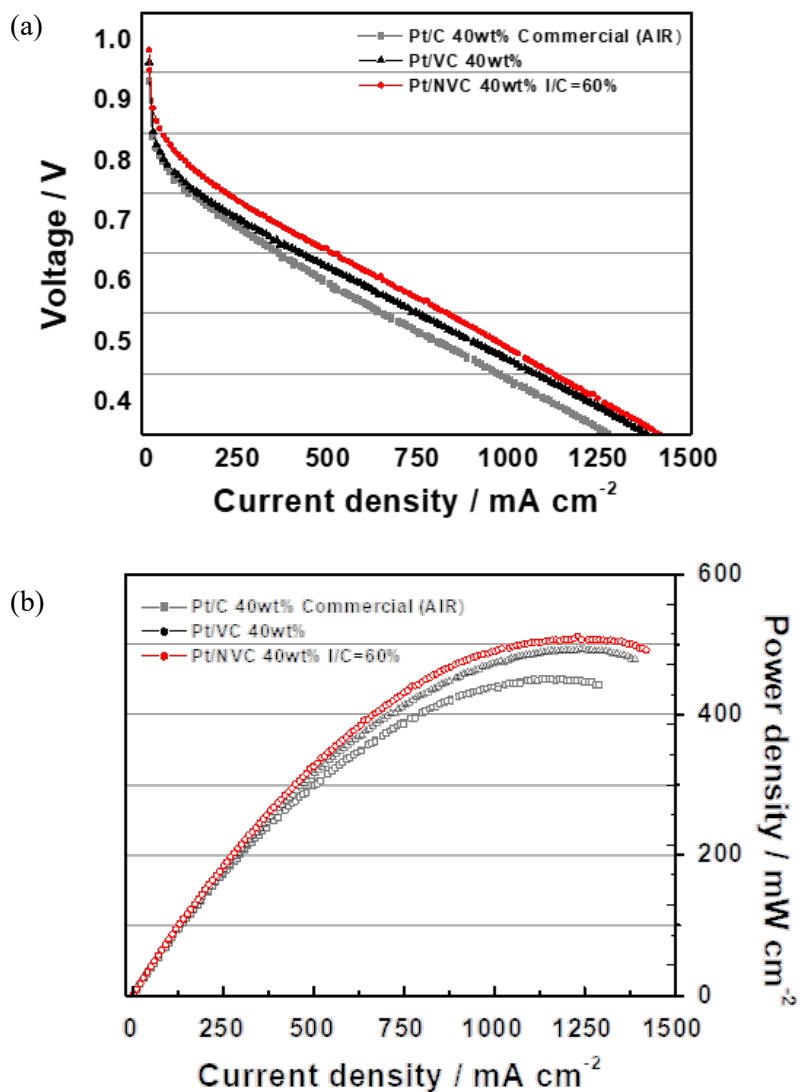
Figure 3.2.4. Current-voltage polarization profile of Pt/NVC 40%, Pt/VC 40%, Commercial Pt/C 40% electrodes (a) voltage profile, (b) power density profile versus current density

Table 3.2.3. Current density of Pt/NVC 40% and Pt/VC 40% electrode MEA (A·cm$_{-2}$) at each polarization region

Div.	0.8V	0.6V	0.4V
Pt/NVC 40%	0.105	0.667	1.266
Pt/VC 40%	0.048	0.585	1.227
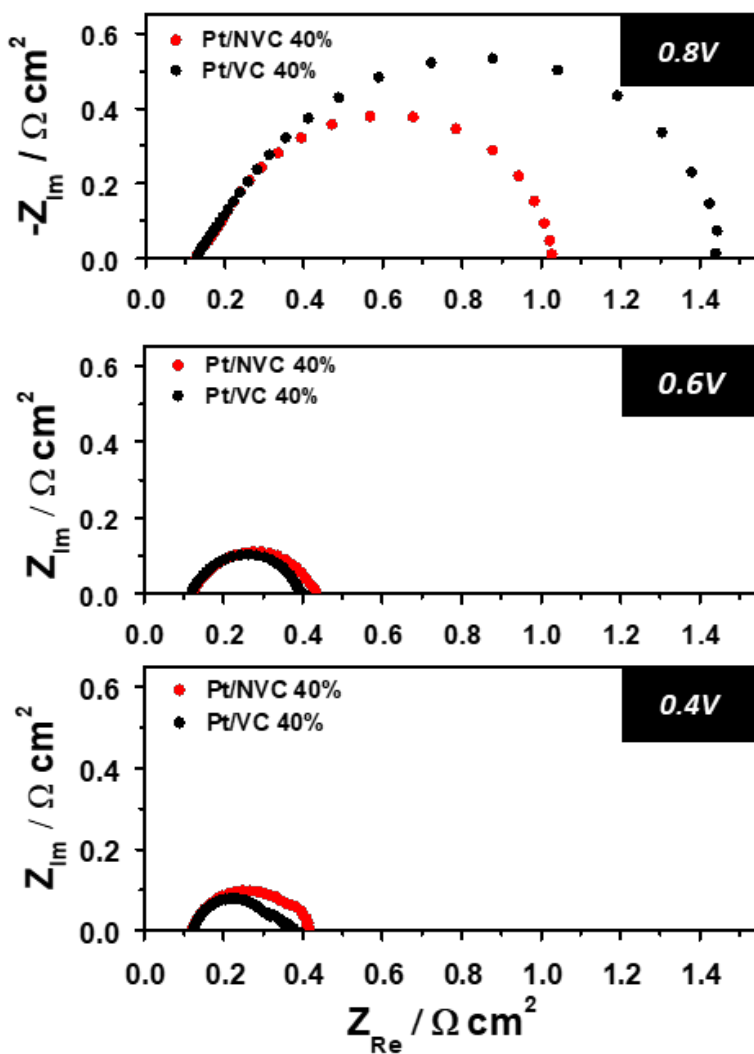
Figure 3.2.5. Electrochemical impedance spectroscopy result of Pt/NVC 40% and Pt/VC 40% electrode MEA

It is clearly seen that the charge transfer resistance is reduced in the activation region from the EIS result in 0.8V. This result is parallel to the observations in the polarization curve. It can be said that the enhanced catalytic activity confirmed from the half-cell test was sell translated to the single-cell level. Another factor that has affected the enhanced performance is expected to have come from the enhanced proton conductivity due to the improvement of catalyst-ionomer interaction and improved ionomer distribution throughout the Pt/NVC 40% electrode. Such hypothesis is further proved by cyclic voltammetry and complex capacitance analysis in the later part.

On the other hand, at 0.6V and 0.4V the impedance of Pt/NVC 40% electrode is slightly larger than that of Pt/VC 40% electrode. Such result is expected to have come from condensed electrode structure shown from reduced cross-sectional thickness and increased hydrophilicity as seen in the previous section.

To see how the electrochemically active surface area (ECSA) has been successfully translated from the half-cell level to single-cell level, cyclic voltammetry result of both levels were compared. The cyclic voltammetry plot and ECSA of the two electrodes calculated from the H_{upd} integrated area is shown in Figure 3.2.6 and Table 3.2.4. respectively.

(a)
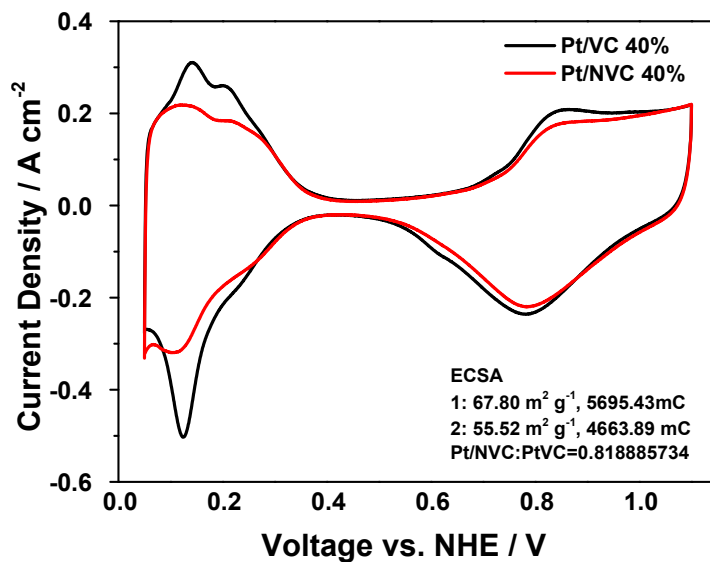
(b)

Figure 3.2.6. Cyclic Voltammetry analysis of Pt/NVC 40% and Pt/VC 40% electrode (a) half-cell level, (b) single-cell level

Table 3.2.4. Electrochemically active surface area translation comparison between two electrodes

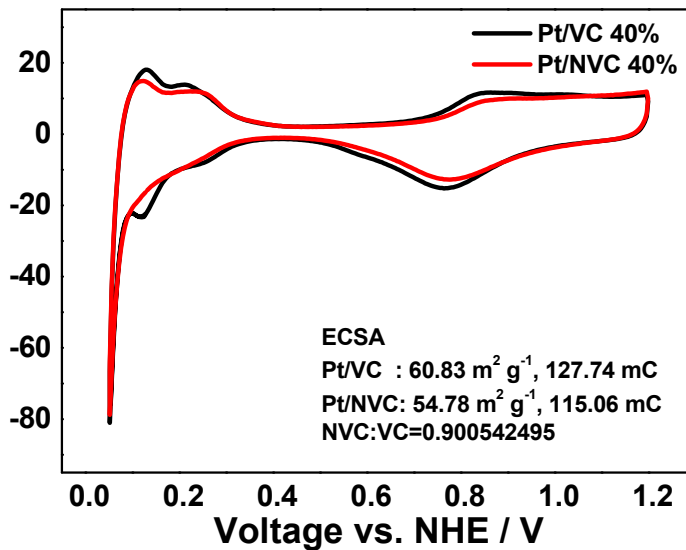| Div.	ECSA ($m^2 g^{-1}$)		Translation ratio
	Half-cell	Single-cell	
Pt/NVC 40%	55.52	54.78	98.67%
Pt/VC 40%	67.80	60.83	89.72%

The translation ratio represents how much the half-cell ECSA was successfully transferred to single-cell. This is important considering the different components of the half-cell and single-cell performance test environments. While proton transport and reactant · product transfer is not a great issue in liquid-electrolyte half-cell, ionomer-catalyst ratio and distribution and the resulting triple-phase boundary is very critical in solid-electrolyte single-cell environment. That 98.67% of the half-cell ECSA was actuated in the Pt/NVC 40% single-cell electrode suggests that the electrode structure and triple-phase boundary formation was extremely successful, considering that only 89.72% of the half-cell ECSA was realized in the case of Pt/VC 40% electrode. Such result was a strong evidence to support the previous hypothesis that the ionomer distribution had been enhanced in the Pt/NVC 40% electrode.

Another electrochemical diagnosis, the complex capacitance analysis, was conducted to determine the proton conductivity of the two electrodes. Complex capacitance analysis allows us to determine the ionic resistance of the electrode by eliminating any faradaic reaction within the cell and considering only the cell inductance, membrane resistance, double layer capacitance, and ionic resistance of the electrode.[44] The experiment was conducted in the same environment as cyclic voltammetry test, feeding H_2 in the anode and inert nitrogen gas in the cathode. The EIS was conducted in

0.45V condition in which barely any faradaic reaction takes place for a Platinum-based electrode. Based on derivations of de Levie on the transmission line model, impedance and complex capacitance can be expressed as below. [45]

$$Z_c(f) = \frac{R_{ion}}{\sqrt{j2\pi R_{ion}C_{dl}f}}\coth[\sqrt{j2\pi R_{ion}C_{dl}f}]$$

$$C_c(f) = \frac{1}{j2\pi f Z_c(f)} = \frac{C_{dl}}{\sqrt{j2\pi R_{ion}C_{dl}f}}\tanh[\sqrt{j2\pi R_{ion}C_{dl}f}]$$

A modified transmission line model suggested by Lim et al. in his PEMFC electrode ionic resistance diagnosis was used in this analysis as shown in Figure 3.2.7.[46] The non-faradaic state EIS result in the form of Nyquist plot is parallel to the capacitance model as shown in Figure 3.2.8, in that the graph starts off with a slope of 45° and reaches a vertical line in the lower frequency region. The complex capacitance analysis could thus be applied to predict the electrode ionic resistance. The modified model allows us to put cell wire inductance (Lw), membrane resistance (R_{PEM}), and charge transfer of the crossovered H_2 gas (R_{X-over}) into consideration and obtain more precise data of electrode ionic resistance. In the experiment procedure no faradaic reaction occurs and thus the electrochemically active sites could be considered as capacitors.
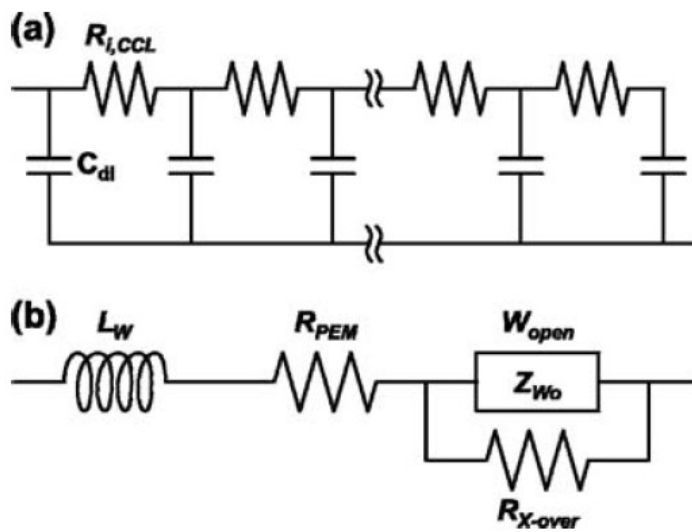
Figure 3.2.7. Traditional transmission line model (a), and the modified traditional transmission line model (b) [46]
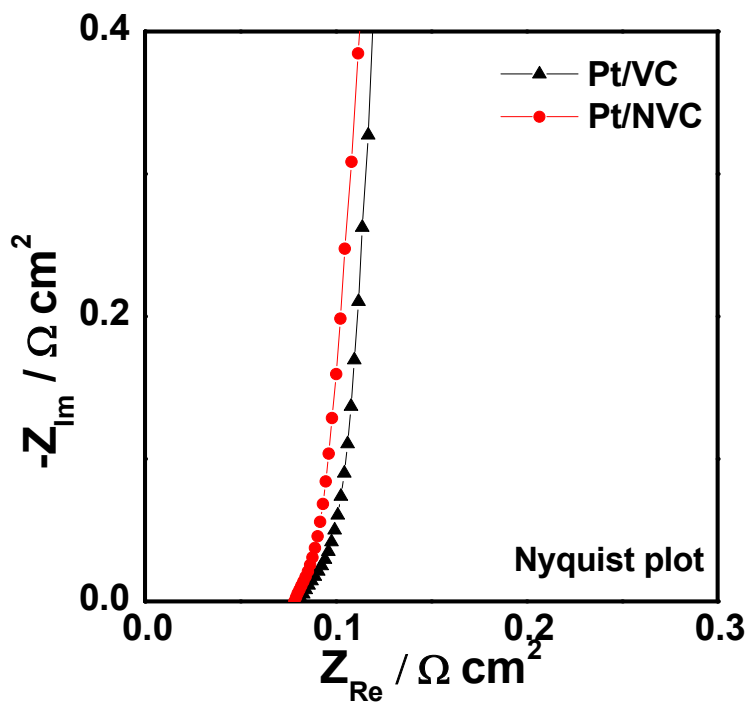
Figure 3.2.8. EIS result of non-faradaic Pt/NVC, Pt/VC electrode in the form of Nyquist plot

The TLM could be further replaced by generalized finite Warburg term for the simplification of fitting and parameters determination ($R_{i,CCL}$ and C_{dl}). The Warburg element (Z_{Wo}) expression is then given by

$$Z_{W_o}(f) = \frac{R}{(j\omega T)^P} coth(j\omega T)^P$$

where $R_{i,CCL}$ represents cathode ionic resistance, C_{dl} is double layer capacitance, ω is angular velocity, j is an imaginary unit, f is AC frequency, and R, T, and P are Warburg element fitting parameters each reflecting uniformity of the electrode, $R_{i,CCL}$, C_{dl}, and $R_{i,CCL}$.[46]

Figure 3.2.8. shows the impedance data in the form of Nyquist plot. It is shown that the impedance graph shows an approximately 0.5 of slope and approaches infinity, showing that the system resembled the behavior of a capacitor in the non-faradaic condition. The complex capacitance could be calculated by the derivations made by de Levie mentioned above. When the imaginary capacitance was plotted against the log of frequency, curves with identifiable peaks could be obtained as shown in Figure 3.2.9. The numerical integration shows that the area of the peak is proportional to double layer capacitance (C_{dl}), and the peak frequency is inversely proportional to $R_{i,CLL}C_{dl}$.[47]

Figure 3.2.9. Imaginary capacitance versus log of frequency for Pt/NVC

40% and Pt/VC 40% electrodes

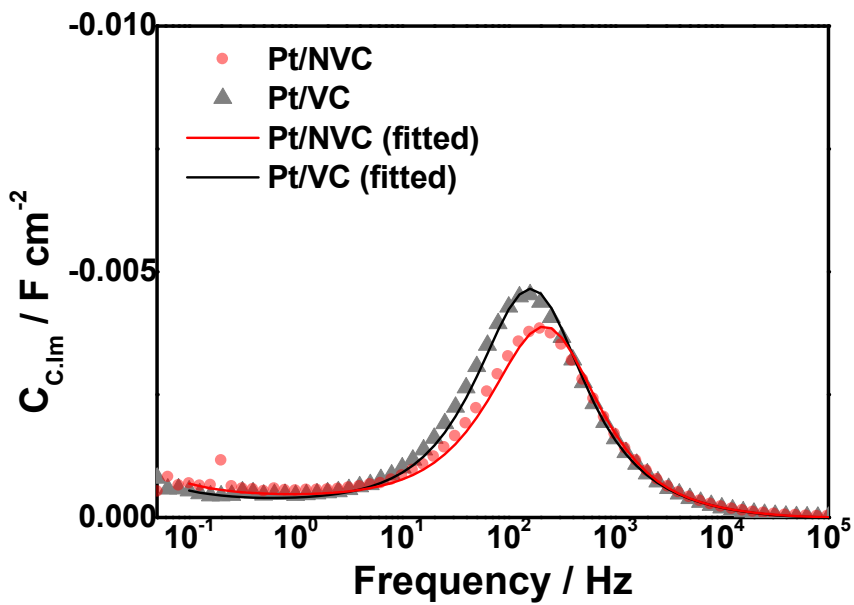The peak area of Pt/NVC 40% electrode was smaller than that of the Pt/VC 40% electrode, while the peak frequency was higher. It could thus be told that the double layer capacitance has decreased for the Pt/NVC 40% electrode, but the comparison on the ionic resistance could not be made. Fitting using the Z-view (Scribner) program of the modified TLM model to the complex capacitance data was thus conducted to numerically compare the ionic resistance of the two electrodes. The fitting parameters and their values are shown in Table 3.2.5. It can be seen that the ionic resistance of the Pt/NVC 40% electrode was determined as 0.04863 while that for Pt/VC 40% electrode was 0.08364. It could thus be concluded that the ionic resistance of the Pt/NVC 40% electrode is superior to that of Pt/VC 40% electrode.

Altogether of the physical and electrochemical analysis on the Pt/NVC 40% and Pt/VC 40% electrode, it could be concluded that the enhanced single-cell performance of the Pt/NVC 40% sample would have come from the combined effect of higher ORR activity of the catalyst and improved electrode structure by enhanced ionomer distribution.

Single-cell behavior in various operating conditions

To test the applicability of the Pt/NVC 40% electrode in various PEMFC operating conditions, variations in relative humidity and backpressure was made and single cell performance in each of the environment was tested.

Table 3.2.5. Fitting parameters of Warburg terms of modified-TLM model

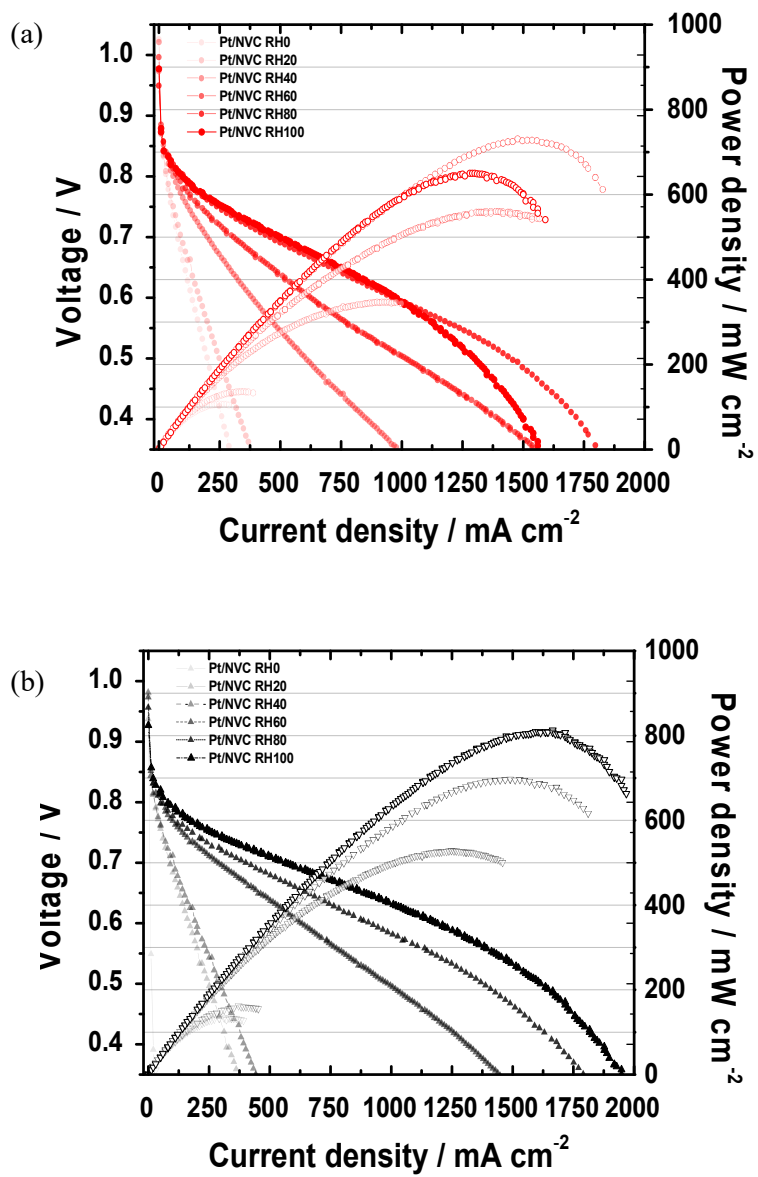| Div.	Warburg element fitting parameters			Double layer
	Z_{WO}-P	Z_{WO}-T / s	Z_{WO}-R / Ω cm^{-2}	C_{dl} / mF cm^{-2}
Pt/NVC 40%	0.4858	0.0003719	0.04863	7.6475
Pt/VC 40%	0.4902	0.0007845	0.08364	9.2794

(a)

(b)

Figure 3.2.10. Single cell performance in various relative humidity conditions (a) Pt/NVC 40% and (b) Pt/VC 40% electrode
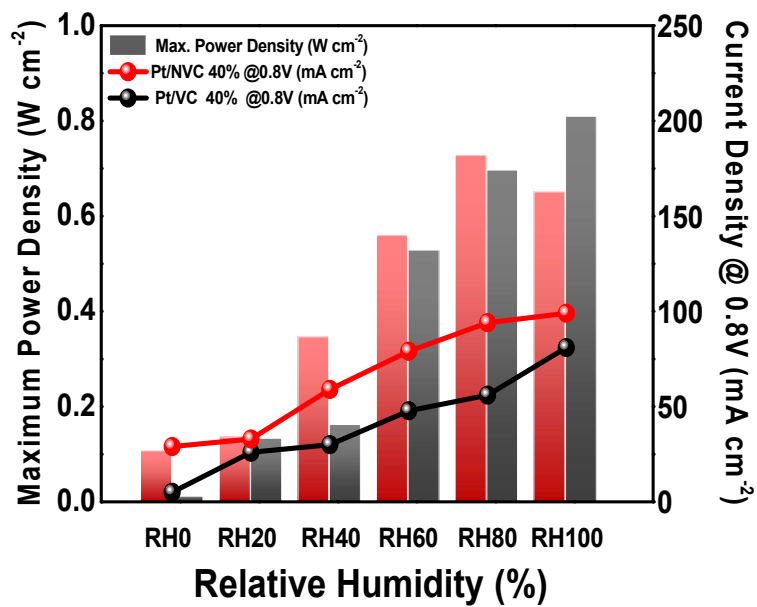
Figure 3.2.11. Comparison of current density in 0.8V and maximum power density in various relative humidity conditions

Figure 3.2.10 shows the single cell performance of Pt/NVC 40% and Pt/VC 40% electrode MEA in different relative humidity conditions separately. To easily compare the performances of two electrodes, graph comparing the current density at 0.8V and maximum power density was plotted. It can be seen that the Pt/NVC 40% electrode outperforms Pt/VC 40% electrode in most of the humidity conditions. However, in a fully humidified condition, the Pt/NVC 40% suffers from reduced maximum power density. This would have come from the fact that the Pt/NVC 40% electrode is more compact and the hydrophilicity has increased compared to Pt/VC 40% electrode. These characteristics is expected to act as disadvantages in water management, increasing mass transfer polarization, and thus reducing the maximum power density.

Backpressure test was also conducted to compare the single-cell performances of the two electrodes. 0.5, 1.0, and 1.5 bar backpressure was applied to both anode and cathode and their performances were recorded as shown in Figure 3.2.12 and 3.2.13. It can be seen and compared from the graphs that the Pt/NVC 40% electrode showed superior performance both in high voltage region and in terms of maximum power density. Such results suggested that the Pt/NVC 40% electrode could be applied to various PEMFC operating conditions with enhanced performance.

(a)
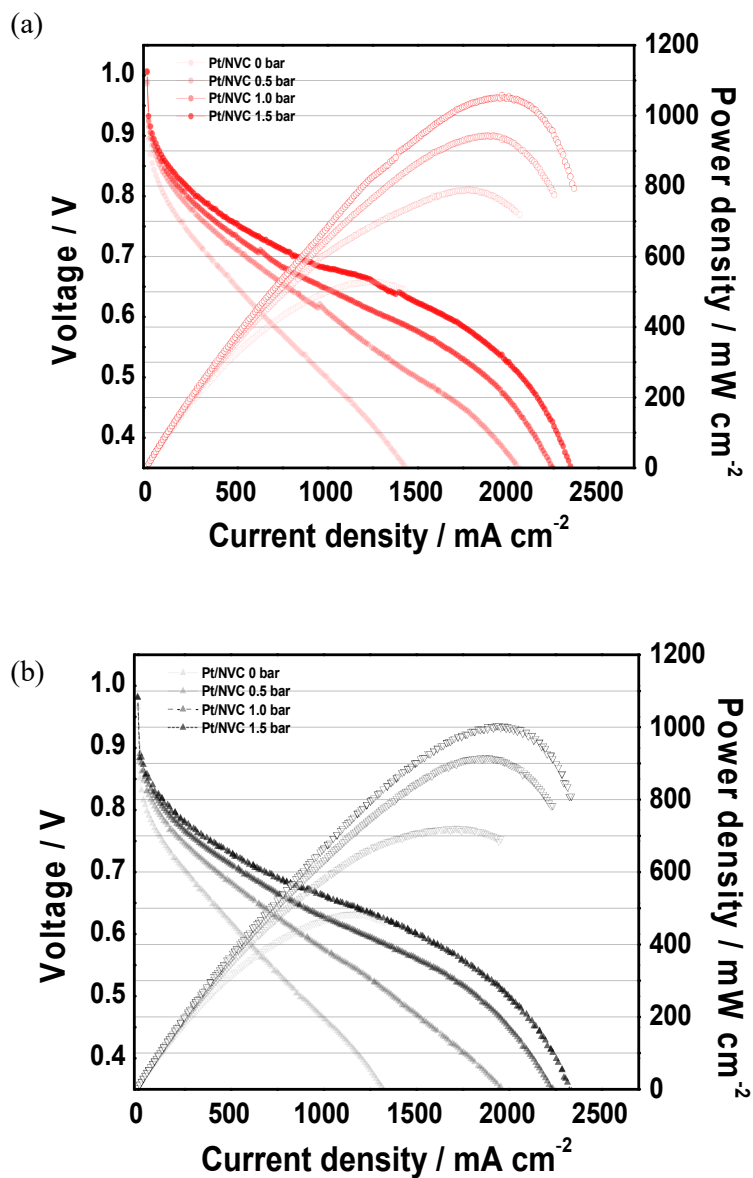
(b)

Figure 3.2.10. Single cell performance in various backpressure conditions (a) Pt/NVC 40% and (b) Pt/VC 40% electrode
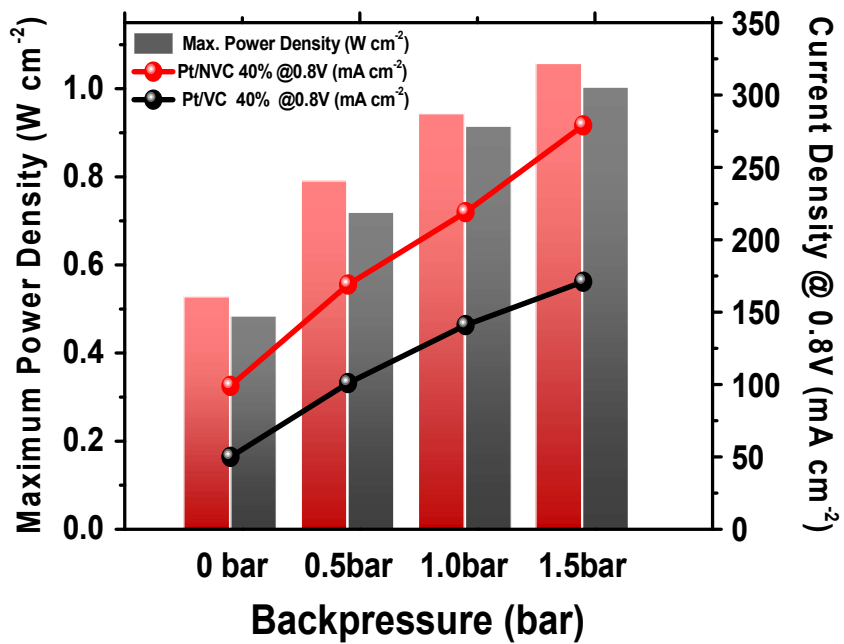
Figure 3.2.11. Comparison of current density in 0.8V and maximum power density in various backpressure conditions

Durability assessment

To test the durability of the two electrodes, i-V cycling for 70 hours was conducted as accelerated stress test (AST). Polarization cycling is considered as one of the harshest stress environment since it covers all the potential range of which different MEA degradation can occur.[48-50]

It can be seen from Figure 3.2.12 that the Pt/NVC 40% electrode was better protected from performance degradation after the AST. The current densities at 0.8V were 0.0379 A cm^{-2} for Pt/NVC 40% and 0.0129 A cm^{-2} for Pt/VC 40% electrode after AST and the maximum power densities were 0.359 W cm^{-2} for Pt/NVC 40% and 0.286 W cm^{-2} for Pt/VC 40% electrode. The performance in terms of both current density at high voltage region and maximum power density was greatly improved in the Pt/NVC 40% as compared numerically.

Electrochemical impedance spectroscopy result as shown in Figure 3.2.13 also shows the superior durability of Pt/NVC 40% electrode. The impedance at 0.8V, representing the activation region, greatly differs between the two electrodes. Such difference was expected to have come from the protection of Pt/NVC 40% catalyst from platinum agglomeration, Ostwald ripening, dissolution and particle detachment. Electrochemically active surface area is thus expected to have better preserved.

(a)

(b)
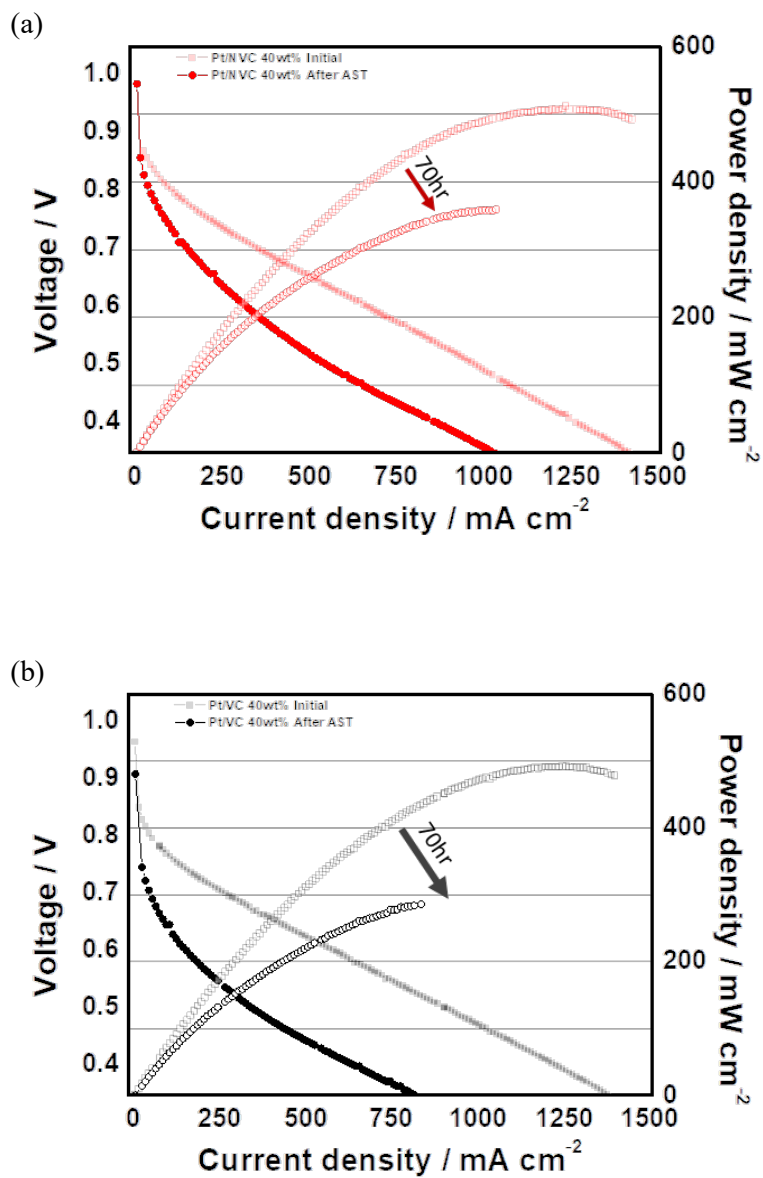
Figure 3.2.12. Single cell performance before and after 70hr AST (a)

Pt/NVC 40% and (b) Pt/VC 40% electrode

Figure 3.2.13. Electrochemical impedance spectroscopy result of Pt/NVC 40% and Pt/VC 40% electrodes after 70hr AST

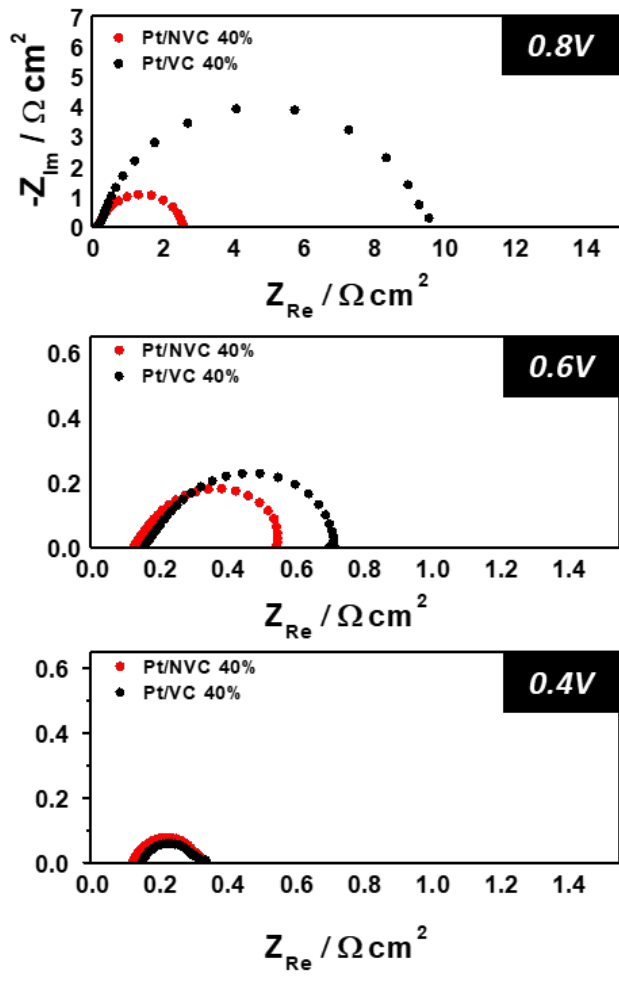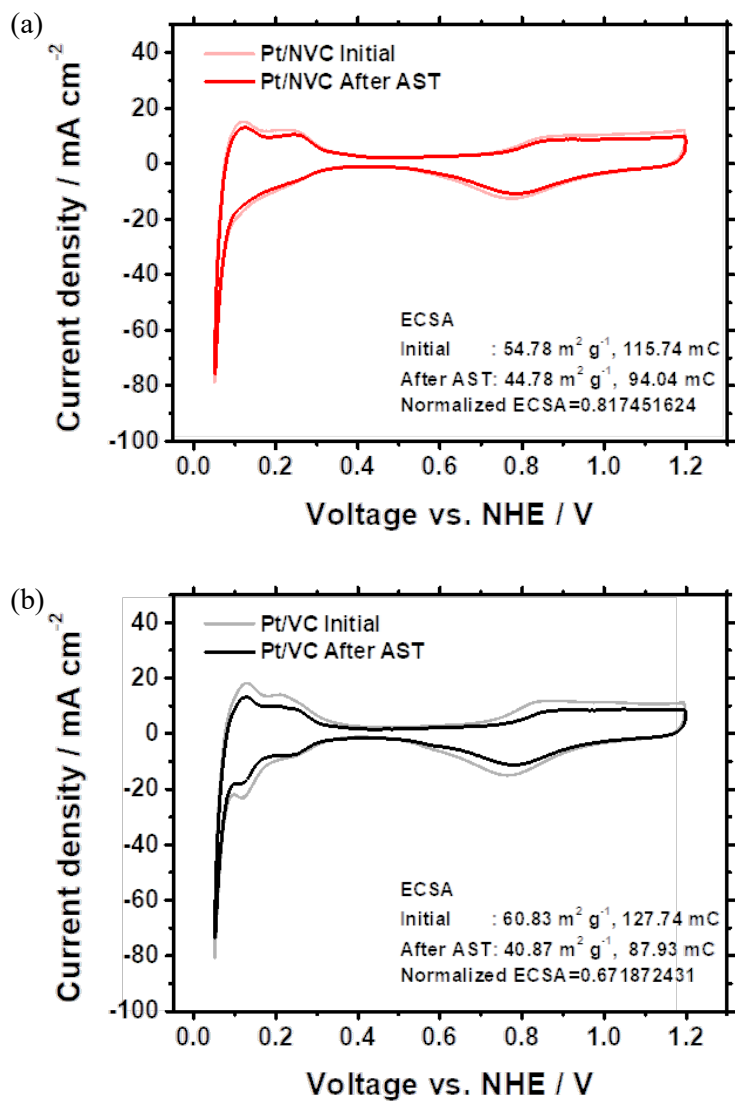**Figure 3.2.14. Cyclic voltammetry analysis before and after 70hr AST**

(a) Pt/NVC 40% and (b) Pt/VC 40% electrode
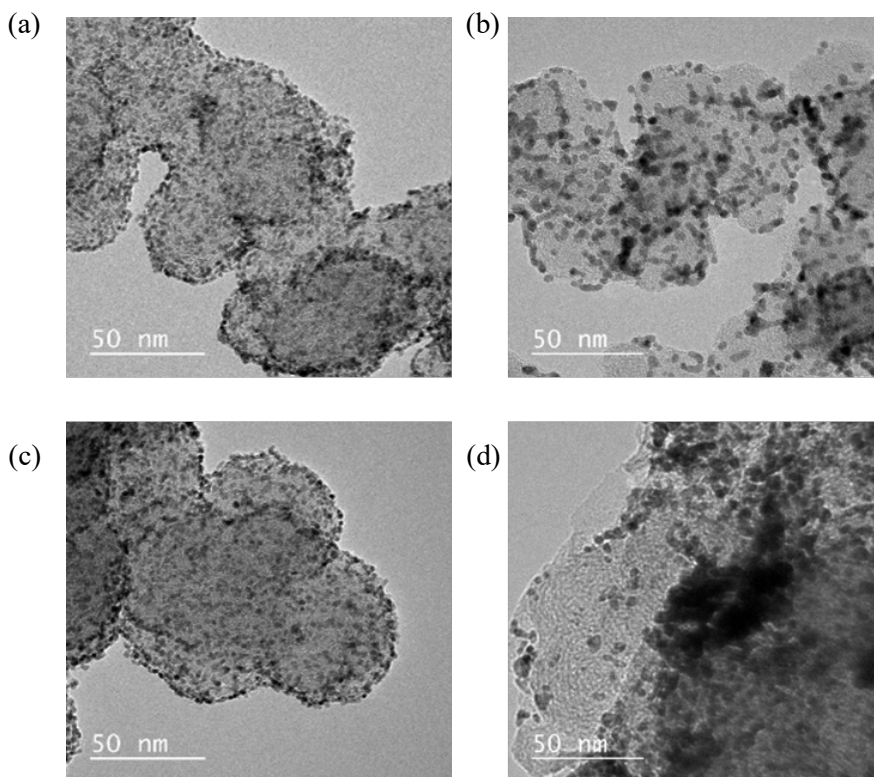
Figure 3.2.15. TEM images of catalyst before and after AST (a) Pt/NVC 40% before AST, (b) Pt/NVC 40% after AST, (c) Pt/VC 40% before AST, (d) Pt/VC 40% after AST

The hypothesis was proven via cyclic voltammetry analysis and TEM analysis of the catalysts after AST. Figure 3.2.14 shows the cyclic voltammetry results of Pt/NVC 40% electrode and Pt/VC 40% electrode single-cell before and after AST. When the ECSA of Pt/NVC 40% electrode decreased from 54.78 m^2 g^{-1} to 44.78 m^2 g^{-1} (81.75%), the ECSA of Pt/VC 40% electrode decreased from 60.83 m^2 g^{-1} to 40.87 m^2 g^{-1} (67.19%). It could be seen from such result that the ECSA was better protected for the Pt/NVC 40% electrode. Physical characterization further proved that the platinum agglomeration and Ostwald ripening was relatively hindered in the Pt/NVC 40%.

Figure 3.2.15 shows the catalysts before and after the AST. From (a) and (c), we can observe the evenly distributed platinum particles in sizes 2-3nm. From (d), it is seen that the Pt/VC catalyst has seriously been deteriorated and the platinum particles either have completely detached or agglomerated in a big chunk. Conversely, although some agglomeration could also be spotted, Pt/NVC 40% catalyst was better protected from degradation. The electrochemical and physical diagnosis on the electrode and catalysts after the AST has confirmed the enhanced durability of the electrode designed with Pt/NVC 40% catalyst.

Chapter 4. Conclusion

In this thesis, the soft-nitriding technique was applied to modify the carbon support of the platinum based catalyst to enhance catalyst activity and single cell performance. The main idea had been to produce a high activity electrocatalyst and successfully translate the enhanced activity to a single cell level, which is crucial to realize the improved fuel cell performance in the actual PEMFC operating conditions.

The catalyst synthesis procedure was established by repeated optimization in both the half-cell and single-cell level. Via liquid-electrolyte half-cell analysis, it was shown that the soft-nitrided Vulcan carbon served as better support to platinum and the ORR activity has improved by almost twofold. Regarding that the platinum loading amount and particle size and distribution were close to identical between the two catalysts, it was shown that by only engineering the carbon support via simple and efficient nitriding method the ORR activity could be maximized.

The electrocatalyst with enhanced property has been applied to MEA by spray coating method and its performance was assessed in the single-cell level. The enhanced performance shown in the performance curve displayed differentiated electrode behavior in each of the polarization regions. The enhanced performance in the high voltage region, representing the activation

polarization region, was expected to have come from not only the enhanced ORR activity but also from the improved ionomer distribution in the Pt/NVC 40% electrode. By performing cyclic voltammetry analysis, it was shown that the ECSA from the half-cell level was better translated for the Pt/NVC 40% electrode and such result was further confirmed by the SEM images of the electrode surfaces. Furthermore, the ionic resistance in the Pt/NVC 40% electrode was proven to have decreased by almost half times by the complex capacitance analysis, which suggested that the enhanced proton conductivity would have worked in combination with the intrinsically enhanced catalytic activity to improve the single-cell performance in the high-voltage region. Although the compromised mass transfer loss increase due to compressed electrode morphology and decreased hydrophobicity, the degree of loss was insignificant in the overall scope since the Pt/NVC 40% electrode outperformed the subjective group in all current regions. Also from the single-cell performance analysis in different relative humidity and backpressure conditions, it could be concluded that the Pt/NVC 40% electrode outperforms the subjective groups in most of the conditions.

The accelerated stress test has further revealed that the platinum particles were better protected from detachment or agglomeration in stressed conditions. The derivations of such improvement can be thought to come from enhanced metal-support interaction due to nitrogen species and

protection of the catalysts in the electrode by coating effect of the well dispersed ionomer. ECSA analysis via cyclic voltammetry and TEM analysis of the catalyst after the AST both proved that the Pt/NVC 40% electrode was enhanced in durability in actual PEMFC operating conditions.

The significance of this study is that the catalyst layer development covered not only the catalytic activity in the half-cell but also the actualization of the improvement in the single-cell level. While many of the research report only the half-cell ORR activity, considerations of the different components in the actual fuel cell operating conditions is very import for the commercialization of the technology. Single-cell diagnosis and optimization result should thus be well reflected to novel electrocatalyst synthesis and optimization procedure. This study has shown that the soft-nitriding technology is well susceptible for performance improvement of the platinum based electrocatalysts supported by carbon and opens a new window for diverse applications in platinum alloy catalysts and more.

References

1. S.-W. C. R. P. O'Hayre, W. Colella, F. B. Prinz, *Fuel cell fundamentals*, John Wiley & Sons, New York, 2006.

2. F. Barbir, *PEM fuel cells: theory and practice*, Academic Press, 2012.

3. Y. Wang, K. S. Chen, J. Mishler, S. C. Cho and X. C. Adroher, *Applied Energy*, 2011, **88**, 981-1007.

4. W. Grove, *Journal of the Franklin Institute*, 1843, **35**, 277-280.

5. P. Costamagna and S. Srinivasan, *Journal of Power Sources*, 2001, **102**, 242-252.

6. H. N. Chen, G. A. Voth and N. Agmon, *J Phys Chem B*, 2010, **114**, 333-339.

7. C. Y. Ahn, M. S. Lim, W. Hwang, S. Kim, J. E. Park, J. Lim, I. Choi, Y. H. Cho and Y. E. Sung, *Fuel Cells*, 2017, **17**, 652-661.

8. P. Y. Chen, C. P. Chiu and C. W. Hong, *Journal of Power Sources*, 2009, **194**, 746-752.

9. S. Litster and G. McLean, *Journal of Power Sources*, 2004, **130**, 61-76.

10. P. Costamagna and S. Srinivasan, *Journal of Power Sources*, 2001, **102**, 253-269.

11.   Q. Shi, C. Zhu, M. H. Engelhard, D. Du and Y. Lin, *RSC Advances*, 2017, **7**, 6303-6308.

12.   H. Schmies, E. Hornberger, B. Anke, T. Jurzinsky, H. N. Nong, F. Dionigi, S. Kühl, J. Drnec, M. Lerch, C. Cremers and P. Strasser, *Chemistry of Materials*, 2018, **30**, 7287-7295.

13.   B. Peter, J. Melke, F. Muench, W. Ensinger and C. Roth, *Journal of Applied Electrochemistry*, 2014, **44**, 573-580.

14.   D. H. Guo, R. Shibuya, C. Akiba, S. Saji, T. Kondo and J. Nakamura, *Science*, 2016, **351**, 361-365.

15.   S. Ott, A. Orfanidi, H. Schmies, B. Anke, H. N. Nong, J. Hubner, U. Gernert, M. Gliech, M. Lerch and P. Strasser, *Nat Mater*, 2020, **19**, 77-85.

16.   A. Orfanidi, P. Madkikar, H. A. El-Sayed, G. S. Harzer, T. Kratky and H. A. Gasteiger, *Journal of The Electrochemical Society*, 2017, **164**, F418-F426.

17.   D. Y. Chung, K. J. Lee, S.-H. Yu, M. Kim, S. Y. Lee, O.-H. Kim, H.-J. Park and Y.-E. Sung, *Advanced Energy Materials*, 2015, **5**.

18.   C.-Y. Ahn, W. Hwang, H. Lee, S. Kim, J. E. Park, O.-H. Kim, M. Her, Y.-H. Cho and Y.-E. Sung, *International Journal of Hydrogen Energy*, 2018, **43**, 10070-10081.

19.   L. Guo, W.-J. Jiang, Y. Zhang, J.-S. Hu, Z.-D. Wei and L.-J. Wan,

ACS Catalysis, 2015, **5**, 2903-2909.

20.   S. Shanmugam, J. Sanetuntikul, T. Momma and T. Osaka, *Electrochimica Acta*, 2014, **137**, 41-48.

21.   F. Hasché, T.-P. Fellinger, M. Oezaslan, J. P. Paraknowitsch, M. Antonietti and P. Strasser, *ChemCatChem*, 2012, **4**, 479-483.

22.   X. Tuaev, J. P. Paraknowitsch, R. Illgen, A. Thomas and P. Strasser, *Phys Chem Chem Phys*, 2012, **14**, 6444-6447.

23.   C. Y. Ahn, J. Ahn, S. Y. Kang, O. H. Kim, D. W. Lee, J. H. Lee, J. G. Shim, C. H. Lee, Y. H. Cho and Y. E. Sung, *Sci Adv*, 2020, **6**.

24.   H. Li, Y. Tang, Z. Wang, Z. Shi, S. Wu, D. Song, J. Zhang, K. Fatih, J. Zhang, H. Wang, Z. Liu, R. Abouatallah and A. Mazza, *Journal of Power Sources*, 2008, **178**, 103-117.

25.   X. Li and I. Sabir, *International Journal of Hydrogen Energy*, 2005, **30**, 359-371.

26.   D. Jeon, *International Journal of Hydrogen Energy*, 2008, **33**, 1052-1066.

27.   A. Ghanbarian, M. J. Kermani, J. Scholta and M. Abdollahzadeh, *Energy Conversion and Management*, 2018, **166**, 281-296.

28.   A. Fly, D. Butcher, Q. Meyer, M. Whiteley, A. Spencer, C. Kim, P. R. Shearing, D. J. L. Brett and R. Chen, *Journal of Power Sources*, 2018, **395**, 171-178.

29. M. Kim, C. Kim and Y. Sohn, *Fuel Cells*, 2018, **18**, 123-128.

30. S. Tanaka and T. Shudo, *Journal of Power Sources*, 2014, **248**, 524-532.

31. M. Arif, S. C. P. Cheung and J. Andrews, *International Journal of Hydrogen Energy*, 2020, **45**, 2206-2223.

32. S. Haji, *Renewable Energy*, 2011, **36**, 451-458.

33. M. G. Santarelli, M. F. Torchio and P. Cochis, *Journal of Power Sources*, 2006, **159**, 824-835.

34. A. A. Kulikovsky, *International Journal of Hydrogen Energy*, 2014, **39**, 19018-19023.

35. X. Huang, presented in part at the IEEE, Montreal, Quebec, Canada, July 9-12. 2006, 2006.

36. M. V. Williams, H. R. Kunz and J. M. Fenton, *Journal of The Electrochemical Society*, 2005, **152**.

37. A. Ganesan and M. Narayanasamy, *Materials for Renewable and Sustainable Energy*, 2019, **8**.

38. J. R. D. Lile and S. Zhou, *Electrochimica Acta*, 2015, **177**, 4-20.

39. D. Banham and S. Ye, *ACS Energy Letters*, 2017, **2**, 629-638.

40. O. H. Kim, C. Y. Ahn, S. Y. Kang, S. Kim, H. J. Choi, Y. H. Cho and Y. E. Sung, *Fuel Cells*, 2019, **19**, 695-707.

41. I. E. L. Stephens, J. Rossmeisl and I. Chorkendorff, *Science*, 2016,

354, 1378-1379.

42. B. Liu, H. Yao, W. Song, L. Jin, I. M. Mosa, J. F. Rusling, S. L. Suib and J. He, *J Am Chem Soc*, 2016, **138**, 4718-4721.

43. J. C. Thurston Herricks, Younan Xi, *NANO LETTERS*, 2004, **Vol. 4**, 2367-2371.

44. J. H. Jang, S. Jeon, J. H. Cho, S.-K. Kim, S.-Y. Lee, E. Cho, H.-J. Kim, J. Han and T.-H. Lim, *Journal of The Electrochemical Society*, 2009, **156**.

45. R. d. Levie, *Advances in Electrochemistry and Electrochemical Engineering*, John Wiley & Sons, New York, 1967.

46. J. W. Lim, Y.-H. Cho, M. Ahn, D. Y. Chung, Y.-H. Cho, N. Jung, Y. S. Kang, O.-H. Kim, M. J. Lee, M. Kim and Y.-E. Sung, *Journal of The Electrochemical Society*, 2012, **159**, B378-B384.

47. J.-H. Jang and S.-M. Oh, *Journal of the Korean Electrochemical Society*, 2010, **13**, 223-234.

48. D. H. a. F. C. Program, *RY2007 Progress Report for the DOE Hydrogen and Fuel Cells Program*, U.S. Department of Energy, Washington, D.C., 2007.

49. X.-Z. Yuan, J. C. Sun, H. Wang and H. Li, *Journal of Power Sources*, 2012, **205**, 340-344.

50. X.-Z. Yuan, S. Zhang, J. C. Sun and H. Wang, *Journal of Power*

Sources, 2011, **196**, 9097-9106.

국문초록

고분자 전해질 연료전지는 수소와 산소의 화학적 에너지를 전기에너지로 변환시켜주는 에너지 변환 장치로 차량용과 발전용으로 널리 사용되고 있다. 수소에너지는 유해물질을 생산해내지 않고 에너지밀도가 높으며 저장성이 뛰어나기 때문에 신재생 에너지 중 가장 미래에너지로 관심받고 있다. 하지만 전기화학반응의 촉매물질로 사용되는 백금의 자원 희소성과 높은 가격이 연료전지의 상용화를 저해하고 있다. 때문에 많은 연구들이 백금 사용량을 줄이면서 산소환원반응성과 내구성을 향상시키는 촉매를 개발하기 위해 진행되고 있다. 가장 최신의 기술로는 전위금속을 이용한 이원합금 등을 코어쉘 구조나 정렬된 구조, 또는 3차원 구조로 합성한 촉매 등이 있다. 이러한 촉매들은 산소환원반응에 큰 발전을 이루며 고분자 전해질 연료전고 상용화에 새로운 가능성을 열고 있다.

하지만 이러한 새로운 촉매들의 전기화학적 성능은 대개 액체 전해질을 사용하는 반쪽전지에서 측정되기 때문에 실제 연료전지 구동환경에서는 제 성능을 발휘하지 못하는 경우가 많다. 이러한 차이는 연료전지의 고체 전해진 사용으로 인한 전극구조, 이오노머 분산도와 두께, 막 수화, 그리고 여러 부품의 저항성에서 나온다. 이러한 차이 때문에 아주 뛰어난 산소환원반응 촉매 성능을 보이는 촉매들도 고체 전해질 단전지에서는 고전하고 있는 경우가 많다. 따라서 새로운 촉매를 설계하고 합성하는 데 있어 단전지상에

서의 촉매의 특성에 대해서 고려할 필요가 있다.

본 연구의 목적은 소프트-나이트라이딩 기법을 활용한 새로운 전기화학적 촉매의 단전지상에서의 특성에 대해 분석하는 것이다. 새로운 촉매를 활용한 막-전극 접합체를 제작하여 실제 연료전지 구동환경에서의 전기화학적 성능을 측정하였다. 그 결과 전반적인 영역에서 향상된 성능을 보인 것을 확인할 수 있었으며, 다양한 물리적 분석과 전기화학적 실험을 통해 향상된 이오노머 분산도가 양성자 전도도 향상에 기여하였으며, 그로 인해 활성화 손실 영역의 성능이 비약적으로 증가한 것임을 확인할 수 있었다. 반면 줄어든 전극 두께와 증가한 친수성의 영향으로 물질전달 손실 영역에서는 다소의 성능 손실을 보였으나, 이 영향은 미미하여 전반적인 성능 향상에 큰 문제가 되지는 않았다. 나아가 다양한 가습, 가압 조건에서도 새로운 촉매가 우수한 성능을 나타내어 다양한 연료전지 가동 조건에서도 적용가능함을 알 수 있었고, 전류-전압 사이클 방식을 활용한 내구성 실험을 통해 향상된 내구도를 증명할 수 있었다.

일련의 실험을 통해 소프트-나이트라이딩을 활용한 새로운 촉매가 실제 연료전지 구동환경에 충분히 적용가능함을 알 수 있었다. 또한 본 연구를 통해 소프트-나이트라이딩 기술이 다양한 백금 기반 촉매에 활용될 수 있다는 가능성을 보여주었으며 이러한 기술을 사용하여 새로운 촉매를 설계하고 전극을 제작함에 있어 고려

해야 할 사항들에 대해 알아볼 수 있었다.

핵심어 : 고분자 전해질 연료전지, 산소환원반응, 질소작용기, 막-
전극 접합체

학 번 : 2018-29625